LBL-22098 c.2
Preprint

Lawrence Berkeley Laboratory
UNIVERSITY OF CALIFORNIA

Materials & Molecular Research Division

RECEIVED
LAWRENCE
BERKELEY LABORATORY

OCT 27 1986

LIBRARY AND
DOCUMENTS SECTION

Submitted to Journal of Chemical Physics

PHOTODISSOCIATION OF CF_2BrCH_2I AT 248, 266, AND 308 nm

T.K. Minton, G.M. Nathanson, and Y.T. Lee

August 1986

TWO-WEEK LOAN COPY
This is a Library Circulating Copy
which may be borrowed for two weeks.

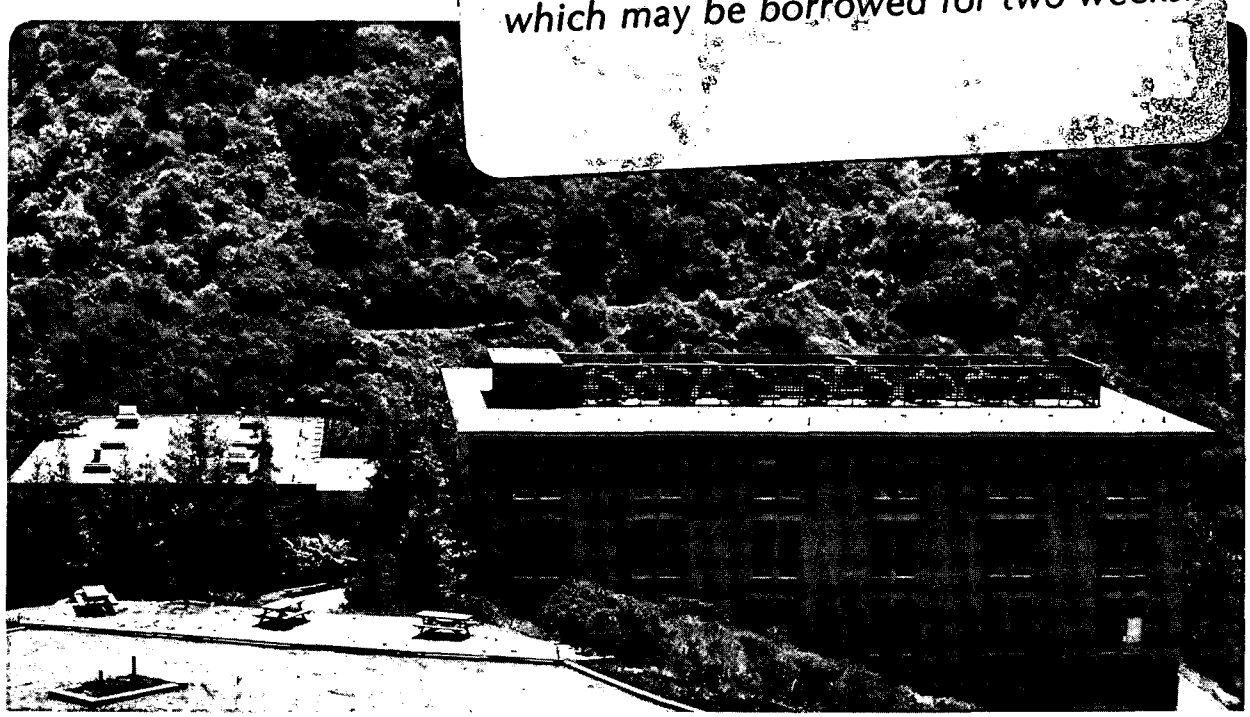

LBL-22098 c.2

Prepared for the U.S. Department of Energy under Contract DE-AC03-76SF00098

DISCLAIMER

This document was prepared as an account of work sponsored by the United States Government. While this document is believed to contain correct information, neither the United States Government nor any agency thereof, nor the Regents of the University of California, nor any of their employees, makes any warranty, express or implied, or assumes any legal responsibility for the accuracy, completeness, or usefulness of any information, apparatus, product, or process disclosed, or represents that its use would not infringe privately owned rights. Reference herein to any specific commercial product, process, or service by its trade name, trademark, manufacturer, or otherwise, does not necessarily constitute or imply its endorsement, recommendation, or favoring by the United States Government or any agency thereof, or the Regents of the University of California. The views and opinions of authors expressed herein do not necessarily state or reflect those of the United States Government or any agency thereof or the Regents of the University of California.

Photodissociation of CF_2BrCH_2I at 248, 266, and 308 nm

Timothy K. Minton,[a] Gilbert M. Nathanson,[b] and Yuan T. Lee

Materials and Molecular Research Division

Lawrence Berkeley Laboratory

and

Department of Chemistry

University of California

Berkeley, CA 94720

ABSTRACT

The technique of photofragmentation translational spectroscopy has been used to study the photodissociation of CF_2BrCH_2I at excitation wavelengths of 248, 266, and 308 nm. The primary photofragments are CF_2BrCH_2 and either $I(^2P_{1/2})$ or $I(^2P_{3/2})$, although some C–Br bond fission does occur at 248 and 266 nm. A large fraction of the CF_2BrCH_2 radical product contains enough internal excitation after the primary process to undergo secondary dissociation into CF_2CH_2 and Br. Secondary dissociation is also observed to take place at 248 and 266 nm via absorption of a photon by the CF_2BrCH_2 photofragment. By observing the threshold for the *spontaneous* secondary dissociation process, the reaction enthalpy for $CF_2BrCH_2I \longrightarrow CF_2CH_2 + Br + I$, was determined to be 67.5±2 kcal/mole, which leads to: $\Delta H^{\circ}_{f,0}(CF_2BrCH_2I) = -92.6\pm2$ kcal/mole. The c.m. translational energy distributions were derived for both the $I(^2P_{1/2})$ and $I(^2P_{3/2})$ dissociation channels resulting from primary C–I bond breakage. The $I(^2P_{1/2})/I(^2P_{3/2})$ branching ratios

---

[a]Present address: Dept. of Chemistry, University of Illinois, Urbana, IL 61801

[b]Miller Fellow

are 3.3, 9.0, and 0.5 for excitation wavelengths of 248, 266, and 308 nm, respectively. The translational energy distributions also reveal that a major fraction of the CF_2BrCH_2 product radicals are formed with high internal energies, averaging around 50% of the excess energy. The angular distributions of dissociation products with respect to the laser polarization indicate that the primary photodissociation process for the ground *and* excited state channels at both wavelengths proceeds via a parallel transition—i.e., the transition moment must be nearly parallel to the C–I bond.

Photodissociation of CF_2BrCH_2I at 248, 266, and 308 nm

I. INTRODUCTION

Photofragmentation translational spectroscopy studies of alkyl iodides[1–9] have yielded detailed information about the partitioning of energy in the photofragments, the branching ratios for the two possible product iodine states, $^2P_{1/2}$ and $^2P_{3/2}$, and the polarization dependence of the product angular distributions with respect to the electric field vector. The number of systems which have been carefully investigated is small, however, and our understanding of the alkyl iodide photodissociation process is still fragmented. Even in the case of methyl iodide, which has been studied extensively[2,3,5] as a prototypical alkyl iodide, detailed analyses have only been completed for two excitation wavelengths in the 200-300 nm region: 248 and 266 nm. Furthermore a magnetic circular dichroism (MCD) experiment,[10] which probed the underlying structure of the $n \longrightarrow \sigma^*$ absorption continuum, could not foretell the predominant spin-orbit state of the I atom product at 248 or 266 nm because of the complication of curve crossing.

According to the prevailing picture,[7] alkyl iodide photodissociation in the 230-310 nm region of the spectrum is assumed to occur via an $n \longrightarrow \sigma^*$ transition localized on the C–I bond. This transition manifests itself as a broad absorption continuum, which was described by Mulliken[11] as consisting of three overlapping bands, with transitions from the ground N state to the ^1Q, $^3Q_1$, and $^3Q_0$ states. An alkyl bromide will exhibit an analogous $n \longrightarrow \sigma^*$ continuum, which will be shifted to shorter wavelength, although still overlapping somewhat with the C–I absorption.[12,13]

In the quest for bond selective photochemistry, photofragmentation studies of CF_2BrCF_2I[7] and CH_2BrI[8,9,13] have been performed in order to discover if excitation in the wavelength region of the C–Br continuum would result in preferential breakage of the stronger C–Br bond over the weaker C–I bond. These studies show that

selective C–Br bond breakage is possible[8] and that the ratio of C–Br to C–I bond fission is dependent on the excitation wavelength as well as the relative orientation of the C–Br bond with respect to the C–I bond in the molecule.

Another iodohaloethane, CH_2ClCH_2I, has also been studied in our laboratory.[6] In addition to the commonly obtainable information (mentioned above), regarding photofragmentation dynamics, we were able to determine the heat of formation of the chloroiodoethane parent, and we could also estimate the C–Cl bond energy of the chloroethyl radical product. These thermochemical quantities could be determined because much of the CH_2ClCH_2 product remained stable after primary C–I bond fission, while a fraction of the radical product was formed with too much internal energy to remain stable and, consequently, underwent secondary decomposition. By finding the center-of-mass translational energy distribution which fitted the stable CH_2ClCH_2 radical time-of-flight signal and by observing the minimum energy in translation at which stable radical could exist, we determined the threshold energy (or reaction enthalpy ΔH) at 0 K for the reaction $CH_2ClCH_2I \longrightarrow CH_2CH_2 + Cl + I$. $\Delta H_f^\circ(CH_2ClCH_2I)$ follows directly from the ΔH for this reaction and $D_0^\circ(CH_2CH_2\text{–}Cl)$ can be inferred by estimating the C–I bond dissociation energy.

Thus far, all the studies of iodohaloethanes have been limited to excitation wavelengths of 248 and 266 nm (except for CF_2BrCF_2I, which was also studied at 193 nm). In general ~50% of the excess energy is observed to appear in translation, and both the ground and excited state iodine (or bromine) channels show a predominantly parallel polarization dependence—i.e., the transition dipole moment must be nearly parallel to the C–I (or C–Br) bond. The branching ratios for $I(^2P_{1/2})$ to $I(^2P_{3/2})$ formation cannot be generalized, however, and they seem to be a function of the individual molecule and excitation wavelength. Besides secondary dissociation of internally excited primary products, which was discussed above, another sec-

ondary process, secondary *photo*dissociation has also been observed to occur when the radical product absorbs a photon and dissociates.[7,8]

In this paper, we report the results of a photofragmentation study of CF_2BrCH_2I in which we explore the dynamics and mechanisms of the primary and secondary photochemical processes occuring at three excitation wavelengths in the $n(\mathrm{I}) \longrightarrow \sigma^*(\mathrm{C–I})$ continuum. A key point in this investigation will be the stability of the CF_2BrCH_2 radical product. This paper is one of several in which we will describe the details of photofragmentation for particular iodohaloethane systems at different wavelengths. After completion of a systematic study of these molecules and a comparison of our results with all the other alkyl iodide studies, we hope that some unmistakable trends will emerge and thus lead to a general understanding of the dynamics of alkyl iodide photodissociation in the $n \longrightarrow \sigma^*$ continuum.

II. EXPERIMENT

Photodissociation of CF_2BrCH_2I was studied at 248, 266, and 308 nm using an apparatus[14] which was designed specifically for the crossed laser and molecular beam technique known as photofragmentation translational spectroscopy.

The apparatus is shown schematically in Figure 1. It consists of a rotatable molecular beam source and a fixed quadrupole mass spectrometer detector in a plane perpendicular to the propagation direction of the laser. The time-of-flight (TOF) signal of the photodissociation products is registered on a 4096 channel multichannel scaler[15] capable of a minimum dwell time of 0.15 μs. Most of our data have been recorded with a 1.0 μs dwell time. The flight path from the interaction region to the electron impact ionizer is 36.8 cm. An important feature of this apparatus is the cold slit mounted in the main chamber near the beam source and facing the detector. This slit is cooled to 25 K, and it reduces the detector background

originating from the main chamber by a factor of 10 because condensible gases will not bounce off the cold surface that is in the viewing window of the detector.

The main resolution limit in the TOF spectra resulting only from the apparatus is determined by the ratio of the effective ionizer length to the flight path length. By observing the extremely fast and monoenergetic H atom fragment from photodissociation of HI at 248 nm and using the minimum 0.15 μs dwell time on the multichannel scaler, we were able to measure the effective ionizer length. Noting that the width in the TOF signal would only be due to the finite length of the ionizer and the laser spot size, we measured a FWHM in the TOF of 0.45 μs peaked at an arrival time of ~20 μs. Using the relation, $\Delta t/t = \Delta l/l$ (for constant velocity), and subtracting the length of the laser spot (0.3 cm), we found an effective ionizer length of ~0.5 cm. Thus, the resolution, due to the finite ionizer length, of a TOF spectrum would be about one part in 75.

In practice, the molecular beam velocity distribution is usually the major limiting factor in the TOF resolution. Our CF_2BrCH_2I beam typically had a peak velocity of 7×10^4 cm/s with a velocity spread (FWHM) of ~12%. We performed velocity distribution measurements by chopping the beam with a spinning disk with four narrow slits (0.075 cm) and observing the TOF of the segments which passed through the slits to the detector. The TOF measurements were fitted with the program, KELVIN,[16] to an assumed form for the velocity distribution, $N(v) \propto v^2 \exp[-(v/\alpha - S)^2]$.[17,18] Table I shows the α and S parameters used for the experiment at each wavelength. The small variations in the velocity distributions for each wavelength were caused mostly by slight differences in the temperature of the nozzle for the different experiments.

The molecular beam was formed by bubbling Ar through liquid CF_2BrCH_2I at 14°C (vapor press. $\approx$ 8 Torr) to yield a total stagnation pressure of 300 Torr. The

mixture was expanded through a 0.125 mm (0.005 in.) dia. nickel nozzle which was heated to 240° -250°C at the tip to prevent dimer formation. The molecular beam passed through two differentially pumped regions before intersecting the laser beam. A skimmer defined the beam to an angular divergence of 3°. The distance from the nozzle to the interaction region was 7.4 cm.

1-bromo-1,1-difluoro-2-iodoethane was custom synthesized by Fairfield Chemical of Blythewood, SC, and it was used without further purification. A GC-mass spectrum showed in our sample a 1% impurity of CF_2BrCH_2Br and a 3% impurity of an isomer, which was determined by NMR to be CF_2ICH_2Br. Only the isomer impurity could potentially cause a problem in the wavelength region of these studies, but we saw no evidence for any interference due to an impurity of this level.

The experiment at 266 nm used the fourth harmonic of a Quanta Ray DCR-1 Nd:YAG laser equipped with a model HG-2 harmonic generator. Following the harmonic generator, the light passed through a Pellin-Broca prism, after which the unwanted fundamental and second harmonic were directed into a beam dump. The fourth harmonic was redirected by a 90° Suprasil I prism into the machine, where it was focused to a spot size of 2.4 mm diameter. In general, the laser output was polarized horizontally—parallel to the detector axis. Occasionally, however, we used the vertical polarization, which was achieved by rotating the harmonic generator by 90°. The laser was adjusted such that the pulse energy in the interaction region was ~30 mJ for both polarizations. At these pulse energies, the Pellin-Broca prism developed tracks, and degradation of the fourth harmonic polarization was observed to become more pronounced as the damage increased. Depolarization interferes with the anisotropy measurements, so we checked the polarization often with a calcite polarizer, and we either moved the prism or replaced it at the first sign of depolarization. We used a crystalline quartz prism and varying quality fused silica

prisms during the experiment, and we found that the fused silica prism purchased from Quanta Ray lasted longest before tracking. Neither the Suprasil I right angle prism nor the MgF_2 lens ever showed any visible damage.

For both the 248 and 308 nm experiments, a Lambda Physik EMG 103 MSC excimer laser was used with the KrF and XeCl transitions, respectively. The optional ILC (Intelligent Laser Control) was used to maintain constant output power. The repetition rate was varied from 100 to 150 Hz. The optical arrangment lay in one plane. The unpolarized output of the laser was directed into a fused silica bending prism which bent the light up at the correct angle into a 60° MgF_2 prism polarizer such that the desired polarization—horizontal or vertical— would come out level and proceed into the machine through a 25 cm fl MgF_2 spherical lens, while the unwanted polarization was blocked. The two polarizations differed in direction by only a few degrees with the vertical component above the horizontal component. The prism polarizer was mounted on a rotation stage so that a simple rotation of the prism would direct the desired polarization, precisely aligned, into the machine. Typical pulse energies at the interaction region for the 308 nm experiment were 12 mJ for horizontal polarization and 18.5 mJ for vertical polarization. The 308 nm spot size was 3 mm wide and 0.4 mm high. At 248 nm, the typical pulse energies were 11 mJ for horizontal and 19 mJ for vertical polarization, and the spot size at the interaction region was 3 mm × 0.6 mm.

At 266 nm, TOF measurements were made at source angles of 10° to 50°. Signal was detected at m/e = 127, 79 (20° only), and 64 (20° only), corresponding to I^+, and Br^+, and $CF_2CH_2^+$, respectively. The respective integrated counts/laser pulse at 20° (horizontal polarization) were 5.5, 2.3, and 0.10. The number of laser pulses was 45,000 for I^+, 100,000 for Br^+, and 280,000 for $CF_2CH_2^+$.

At 248 nm, TOF measurments were made at source angles of 20° to 50°. Sig-

nal was detected at $m/e = 127(I^+)$, $79(Br^+)$, and $64(CF_2CH_2^+)$. I^+ TOF's were counted for 100,000 laser pulses with a count rate (horizontal pol.) at 20° of 1.3 counts/pulse. Br^+ was counted only at 20° for 200,000 pulses with a count rate of 0.81 counts/pulse. $CF_2CH_2^+$ also was counted only at 20° for 1,000,000 pulses with a count rate of 0.28 counts/pulse.

At 308 nm, signal was detected at two masses—$127(I^+)$ and $79(Br^+)$. I^+ TOF's were recorded at source angles of 10° to 50° for 200,000 laser pulses with a count rate (horizontal pol.) at 20° of 0.14 counts/pulse. Br^+ was recorded only at 20° for 1,000,000 pulses with a count rate of 0.12 counts/pulse.

In all three experiments, we made an unsuccessful effort to observe the parent CF_2BrCH_2 radical at $m/e = 143$. The only mass which showed any evidence of stable radical was $m/e = 79(Br^+)$. This mass is not ideal for observing stable radical (through dissociative ionization) because most of the Br^+ signal is expected to result from atomic Br, which is present at high levels because of secondary decomposition of CF_2BrCH_2 product.

In general, two types of angular distributions were performed. The signal was monitored as a function of source angle for fixed horizontal polarization, and the signal was monitored for horizontal and vertical polarizations at a fixed angle. The exception for the latter case was at 266 nm, where the polarization could not be changed without realigning the laser beam. For both types of angular dependences, the angle or the polarization was changed often and the scan repeated many times to offset any drifts which might have occured in the laser power, the electronics, or the molecular beam intensity.

The 248 and 266 nm laser intensities were high enough that saturation could affect the angular distributions. (The effect of saturation will be discussed in Section IV.) In order to ascertain the amount of saturation, we took an absorption

spectrum of gaseous CF_2BrCH_2I on a Cary 14 spectrophotometer (Figure 2) to determine the absorption cross section. Table II gives the cross section as well as the product of the cross section and laser intensity for each wavelength studied.

III. RESULTS AND ANALYSIS

The goals of the data analysis are the center-of-mass (c.m.) product translational energy distribution $P(E_T)$ and the determination of the parameter β in the c.m. angular distribution, expressed in the form[19(b)]

$$w(\theta) \propto 1 + \beta P_2(\cos\theta), \tag{1}$$

where θ is the angle between the electric vector of the laser light and the c.m. recoil direction of the products. The calculated c.m. flux distribution is assumed to be the product $P(E_T)w(\theta)$. The primary data, from which the $P(E_T)$ and β are derived, are the laboratory TOF distributions $N(t)$ and the laboratory angular distributions $N(\Theta)$. For a single photon dipole transition to a repulsive state in a diatomic molecule, the anisotropy parameter β is related to the angle α between the transition moment and the bond dissociation coordinate according to [19(b)]

$$\beta = 2P_2(\cos\alpha). \tag{2}$$

For a purely parallel transition, $\alpha = 0°$, $\beta = 2$, and $w(\theta)$ is a $\cos^2\theta$ distribution, while for a purely perpendicular transition, $\alpha = 90°$, $\beta = -1$, and $w(\theta)$ is a $\sin^2\theta$ distribution. For polyatomic molecules, however, several physical effects, involving motion of the excited molecule prior to dissociation, are often imbedded in β. Saturation in the laser excitation can also affect β, and this saturation effect is taken into account in the analysis using a model first proposed by Ling and Wilson[20] (see Discussion).

The $P(E_T)$ and β are determined by a forward convolution technique in which a $P(E_T)$ distribution and a β are guessed and then convoluted with the beam velocity distribution, ionizer length, and laser spot size. A c.m. to lab transformation is then performed, yielding a calculated $N(t)$ distribution which is compared to the observed TOF. The $P(E_T)$ and β are refined until a satisfactory fit is simultaneously obtained for all TOF and angular distributions. We have found empirically that including in our fitting routine the 3° angular divergence of the molecular beam and the 1.5° angular divergence of the detector aperature will only negligibly narrow the fitted $P(E_T)$ distribution.

The TOF distributions presented here show the total time for a fragment to go from the interaction region to the ionizer, and after ionization, through the quadrupole mass filter to the Daly-type ion counter. The true flight time from the interaction region to the ionizer is found by subtracting the ion flight time from the observed total arrival time. The ion flight time for a singly charged ion of mass m has been found experimentally, and it can be expressed in μs by the formula $\alpha\sqrt{m}$ where the parameter α is a function of the ion energy, the resolution, and other mass spectrometer parameters. α was equal to 3.96 for all of the data reported here with the exception of the iodine TOF's at 266 nm, where α was determined to be 2.64.

A. TOF and angular distributions

1. 266 nm

Figure 3 shows the iodine fragment TOF data for horizontal polarization at various angles along with the best calculated fits using the $P(E_T)$ in Figure 15. (The two components fit separately were deconvoluted such that the two curves would be smooth and unimodal.) Three components are definitely present in the TOF. Based

on previous alkyl iodide studies,[1-9,22-24] we would have expected two components arising from two dissociation pathways: one yielding faster, ground state $I(^2P_{3/2})$, and the other yielding slower, spin-orbit excited $I(^2P_{1/2})$. Indeed, the two most prominent peaks in the TOF are consistent with the previous observations[6,7] that about half the available energy for each channel appears in translation—see the $P(E_T)$ in Figure 15. The third slow component is associated with primary C–Br bond fission and originates from the CF_2CH_2I fragment (see below and part B).

The angular distribution for fixed horizontal polarization is shown in Figure 4. For reference, two fits are shown for different values of β. It is apparent that the angular distribution is not very sensitive to β, although the range of β's that fit the angular distribution is indicative of a predominantly parallel transition. Figure 5 shows a kinematic diagram for CF_2BrCH_2I photodissociation with I atom detection, where it can be seen that the recoil velocities are large enough compared to the beam velocity that $\cos^2\theta$ does not change much over the range of c.m. angles sampled for a given laboratory angle (when using horizontal polarization). Thus, the shape of the calculated $N(t)$ distribution is mostly sensitive to the $P(E_T)$ distribution, while the shape of the calculated $N(\Theta)$ distribution is mostly sensitive to β. It is a fortunate circumstance that the $P(E_T)$ and β can be optimized almost independently. As is also seen in Figure 5, when the laser polarization is vertical, $\cos^2\theta$ for the complementary c.m. angle does change significantly over the range of a TOF distribution. Consequently, fitting a vertical polarization TOF after finding the correct $P(E_T)$ from a horizontal polarization TOF provides a double check on β. Experience has shown that we can only expect to be accurate to about ± 0.3 in β with the fixed polarization method of measuring the angular dependence. A rotating detector machine, which has been used in our laboratory for other similar experiments,[6,7] is much better suited for such angular studies, as the c.m. angle

changes dramatically over the range of a typical angular distribution. On the other hand, the geometry of the rotating source apparatus is much better (in fact necessary) for angular distributions obtained by rotating the laser polarization at fixed beam angles, which provide, in theory, a very sensitive determination of β.

We did perform a fixed beam angle, horizontal/vertical polarization dependence at 266 nm, but we were not able to repeat the measurement over and over to average out drifts. As mentioned in Section II, when we rotated the polarization, the laser had to be realigned. Nevertheless, we were careful to use the same alignment, laser power, and experimental conditions for measuring the signal with each polarization. The anisotropy parameter given by this angular dependence was 1.6. Table III shows the sensitivity of the calculated horizontal to vertical polarization signal ratio in the determination of β.

A final test of β comes from fitting the vertical polarization, iodine TOF at 20°. Figure 6 shows the data with the calculated fits for a given $P(E_T)$ and three different β parameters. $\beta = 1.6$ gives the best fit, but the other fits are not bad. Based on the preponderance of the evidence, we will take $\beta = 1.6 \pm 0.2$ as the anisotropy parameter for the 266 nm photodissociation process. It should be noted that we tried fitting the data using two and three different β values for the different components in the TOF (by arbitrarily deconvoluting the $P(E_T)$), and we were forced to conclude that all three components have the same anisotropy.

An incidental feature in Figure 6 is the long slow tail, which was not present in the horizontal polarization TOF data. This tail is caused by a small amount of clusters in the beam. Vertical polarization (i.e., when the electric vector is perpendicular to the detector axis) accentuates signal from clusters because their slow c.m. velocities make their detection possible only at large c.m. angles; thus, assuming a parallel transition, the more favorable polarization would be vertical. Apparently,

even the heated nozzle did not prevent some clusters from forming.

We observed a TOF spectrum at $m/e = 79(Br^+)$ in addition to the iodine data. Figure 7 shows this TOF distribution along with a section of the same distribution on an expanded scale. Included also is the calculated fit for the stable CF_2BrCH_2 fragment assuming it would be seen at $m/e = 79$. Based on CH_2ClCH_2I photodissociation,[6] the radical fragments are expected to be internally hot, with a large fraction of the CF_2BrCH_2 radicals undergoing secondary dissociation into CF_2CH_2 and Br. The observed broad TOF is suggestive of secondary dissociation, while the fast feature probably contains an additional contribution from primary C–Br bond fission. At ~300 μs, a small peak is discernable, and because it falls in the range of the calculated CF_2BrCH_2 TOF, it is probably an indication of a small amount of stable CF_2BrCH_2 product.

With the observation of stable difluorobromoethyl product as a goal, we searched in vain for signal at the parent mass, 143. Apparently, even if stable radical were formed, it did not survive electron bombardment in the ionizer. Another possible mass for observing the stable CF_2BrCH_2 product was $m/e = 64(CF_2CH_2^+)$. The measured TOF in Figure 8 does not exhibit any definite feature at the expected stable radical arrival time, although there is a hint of a peak at ~300 μs, which corresponds exactly to the arrival time of the small, stable radical peak in the Br^+ TOF (when the proper correction for ion flight time is made). Unfortunately, the signal-to-noise ratio of the data is not very good because we had to increase the mass spectrometer resolution to filter out the I^{++} signal at $m/e = 63.5$. Nevertheless, the characteristically broad secondary dissociation signal is present as well as a fast peak, which, by conservation of energy, must result from secondary *photo*dissociation, where the radical has absorbed another photon and fallen apart with a large translational energy release. The Br^+ TOF distribution should also

show this fast, secondary photodissociation signal, and we can estimate by conservation of momentum that secondary photodissociation accounts for the signal under the fast edge of the sharp feature in the Br^+ TOF.

2. *248 nm*

The iodine TOF spectra, shown in Figure 9, from 248 nm photodissociation are similar to those seen at 266 nm. As before, three components are clearly visible, with the fast ground state iodine peak more prominent in the 248 nm TOF's. While the ground and excited state iodine channels could not be resolved completely in the time-of-flight, we separated the $P(E_T)$ into two components, as we did for the 266 nm data (see Figure 15), and the fits are shown in Figure 9.

As usual for the experiments on the rotating source apparatus, the fixed polarization-rotating source angular dependence did not give a distribution which was very sensitive to the β parameter, and we could find one $P(E_T)$ along with a range of β values, from 1.0-2.0, which would satisfactorily fit all the iodine TOF's as well as the angular distribution. However, at 20° we collected I^+ data at both horizontal and vertical (Figure 10) polarizations, and a simultaneous fitting of the shape of the two TOF spectra was very dependent on the β parameter as well as the $P(E_T)$ distribution. We were able to fit the horizontal and vertical polarization TOF's simultaneously, provided the $I(^2P_{1/2})$ fraction in the $P(E_T)$ was 0.77 and the $I(^2P_{3/2})$ fraction was 0.23 *and* provided the ground state β was 0.35 lower than the excited state β. We also tried arbitrarily separating the $P(E_T)$ to give a third component, corresponding to the slow shoulder, but we concluded that it must have the same anisotropy as the excited state iodine channel. The relation between the two β values was thus established, but their actual values could still not be resolved.

The horizontal/vertical polarization dependence on the integrated signal fur-

nished the final constraint needed to determine the anisotropy paramenters. Table IV shows the calculated horizontal to vertical polarization signal ratios for selected β values in addition to the experimental ratio. (Note that all the ratios in Table IV include the effect of laser saturation.) The best fit β pair is $\beta^* = 1.6$ and $\beta = 1.25$, and these are the parameters used in the fits in Figures 9 and 10.

Figure 11 shows the bromine TOF distributions recorded for both horizontal and vertical polarizations. The two TOF's are strikingly different in the intensity of the fast feature with respect to the broad secondary background. This fast peak is presumably a combination of Br^+ arising from secondary photodissociation of the CF_2BrCH_2 radical and, more importantly, primary photodissociation resulting in C–Br bond cleavage. The peak of the fast feature in both the 248 and 266 nm Br^+ TOF distributions occurs at an arrival time which can be explained by assuming Br formation with ~1/2 the available energy going into translation—a common observation in C–I bond fission.

The fact that the fast bromine peak decreases markedly, relative to the broad background, on going from horizontal to vertical polarization is suggestive of a primary process with a parallel polarization dependence. The secondary signal originates from decomposition of the relatively slow CF_2BrCH_2 radical, which will show a less sensitive polarization dependence than the fast Br product from C–Br bond dissociation, because the c.m. angle changes less between horizontal and vertical polarization for a slower product than for a faster product (at a given laboratory angle).

From the fast secondary photodissociation peak in the $CF_2CH_2^+$ TOF (Figure 12), the peak arrival time of the complementary bromine signal can be estimated to be ~235 μs. Thus, the secondary photodissociation signal is under the fast side of the prominent peak in the Br^+ TOF. This conclusion is consistant with

B. Product translational energy distributions and branching ratios

The fits to the TOF and angular distributions were calculated using the $P(E_T)$ distributions shown in Figure 15. In each case, the $P(E_T)$'s for the ground and excited state iodine dissociation channels were not completely resolved, so the dashed curves represent our best estimates for their separation. It is more difficult to separate the slow shoulder from the $I(^2P_{1/2})$ $P(E_T)$ for 248 and 266 nm photodissociation, but we have done so in order to illustrate the approximate shape of the excited state iodine component.

An energy level diagram for C–I and C–Br bond fission in CF_2BrCH_2I is shown in Figure 16. The energy available for translation and internal excitation of the products (E_{avl} for $^2P_{3/2}$ and E^*_{avl} for $^2P_{1/2}$ formation) is given by the energy conservation expressions,

$$\begin{aligned} E_{avl} = h\nu + E^P_{int} &- D^\circ_0(\text{C–I[Br]}) = E_T + E^R_{int} \\ E^*_{avl} &= E_{avl} - E_{so}, \end{aligned} \tag{3}$$

where E^P_{int} is the part of the initial internal energy, which is stored in the vibrational degrees of freedom of the CF_2BrCH_2I parent that are directly coupled to the dissociation coordinate, and E^R_{int} is the internal energy of the radical fragment after photodissociation. D°_0(C–I) is estimated to be 55.8 ± 1.5 kcal/mole, and D°_0(C–Br) is estimated to be ~68 kcal/mole (see Discussion, part B). The photon energy $h\nu$ is 115 kcal/mole at 248 nm, 107.5 kcal/mole at 266 nm, and 92.8 kcal/mole at 308 nm. E_{so}, the $^2P_{3/2}$ - $^2P_{1/2}$ spin-orbit splitting is 21.7 kcal/mole for I and 10.59 kcal/mole for Br.

As mentioned in part A, a small peak attributable to stable CF_2BrCH_2 radical is observed in the bromine TOF at 266 nm. Unfortunately, the stable CF_2BrCH_2 radical peak was of much too poor quality to fit (unlike the analogous stable CH_2ClCH_2

radical peak in the previous CH_2ClCH_2I experiment[6]), so we performed a simple calculation of the translational energy with the use of a kinematic (Newton) diagram (e.g., Figure 5) and the assumption of a monoenergetic molecular beam and infinite detector resolution. By carrying out this calculation for various points over the range of the peak, we obtained an idea of the accuracy of our method. Fortunately, the peak was very narrow, and over half the width of it (the slow half), the c.m. translational energy changed from 16.5 to 20 kcal/mole. Because the peak is so narrow, all the CF_2BrCH_2 radicals formed must be near their maximum internal energy (i.e., near the C–Br bond dissociation limit). Thus, we take the midpoint, 18.3±2 kcal/mole, as the translational energy threshold.

This threshold energy provides the information necessary to calculate the change in enthalpy ΔH for the reaction,

$$CF_2BrCH_2I \longrightarrow CF_2CH_2 + Br + I. \tag{4}$$

From Equation (3), ΔH for this reaction can be determined [assuming $E^P_{\rm int}$ is equal to zero (see Section IV. B.)] as follows:

$$D^\circ_0(CF_2BrCH_2 - I) + D^\circ_0(CH_2CF_2 - Br) = h\nu - E_{so} - E_T(\min), \tag{5}$$

where $D^\circ_0(CH_2CF_2\text{–}Br)$ has been used instead of $E^R_{\rm int}(\max)$. ΔH (at 0 K) for reaction 4 is then 67.5 ± 2 kcal/mole.

The slowest component in the iodine TOF at 248 and 266 nm can be understood in light of the result above. Based on C–Br bond energies for similar bromoethanes (see Table VII), we know that ΔH (at 0 K) for the reaction,

$$CF_2BrCH_2I \longrightarrow CF_2CH_2I + Br, \tag{6}$$

is 67-68 kcal/mole. Since the C–Br bond dissociation energy is almost the same as the energy required to break both the C–Br and C–I bonds, $D^\circ_0(CF_2CH_2\text{–}I)$

must be approximately 0 kcal/mole. If we assume that primary C–Br bond fission occurs and that the slow shoulder is the result of the CF_2CH_2I product, and if we assume that Br is formed in the spin-orbit excited state, then the energy available for translation at 248 nm is 115 – 69 – 10.6 = 35.4 kcal/mole, and at 266 nm, the available energy is 107.5 – 69 – 10.6 = 27.9 kcal/mole. The peak of the slow bump corresponds to a c.m. translational energy of ~32.5 kcal/mole at 248 nm and ~27 kcal/mole at 266 nm. Therefore, the CF_2CH_2I internal energy is about 3 kcal/mole at 248 nm and about 1 kcal/mole at 266 nm. These values are, of course, subject to error because of the uncertainty in the peak position and in the C–Br bond energy; nevertheless, they fall in the range of the expected bond energy of the radical. Whether the CF_2CH_2I radical is stable or not, it can account for the slow bump because even if it is unstable by one or two kcal/mole, the iodine will be recoiling from the CF_2CH_2 relatively slowly compared to the initial velocity of the CF_2CH_2I product. Hence, the I^+ TOF signal from secondary dissociation of slightly unstable CF_2CH_2I would appear similar to the I^+ TOF signal from a slightly stable CF_2CH_2I product. Ground state Br formation would not lead to a distinct bump in the TOF, because the higher available energy would cause the two secondary fragments to recoil from each other with a broad range of velocities. In summary, the slow bump is consistent with a $D_0^\circ(CF_2CH_2\text{–}I)$ of approximately 0 kcal/mole, but we cannot conclude from our data whether or not the CF_2CH_2I radical is weakly chemically bound.

From the areas under the $P(E_T)$ distributions, we can estimate branching ratios for the formation of the two electronic states of iodine. The $I(^2P_{1/2})/I(^2P_{3/2})$ ratios are 3.3, 9.0, and 0.5, respectively for 248, 266, and 308 nm. These results do contain uncertainties, mainly resulting from the deconvolution of the curves. Other errors can arise from the noise in the data, which leads to ambiguities in the fits. Despite

the uncertainties, our ratios are probably accurate to 10%.

Finally, we compare the fraction of the available energy that went into translation for the average E_T and the extremes in the $P(E_T)$ distribution. The results are summarized in Table VI.

IV. DISCUSSION

A. Anisotropy and polarization

The polarization dependences of both the ground and excited state iodine channels at all three wavelengths studied suggest a predominantly parallel transition for every photodissociation process observed. However, the anisotropy parameter β is, in every case, less than 2, the expected β value for a purely parallel transition. We will examine below the factors that can reduce β, and we will estimate the relative importance of each.

Rotation of the excited complex prior to dissociation would cause a reduction in β if the excited state lifetime were long enough to allow the molecule to rotate such that the recoil direction of the products differed significantly from the initial orientation of the C–I bond. Following a derivation by Jonah[21] and also Busch and Wilson,[19(b)] the angular distribution arising from dissociating molecules with a random distribution of lifetimes is

$$w(\theta) \propto 1 + \beta_{true} \left[\frac{1 + (\omega\tau)^2}{1 + 4(\omega\tau)^2} \right] P_2(\cos\theta), \tag{7}$$

where the observed β_{obs} would be the true β_{true} reduced by the factor $[1+(\omega\tau)^2]/[1+4(\omega\tau)^2]$, and $\omega\tau$ is the angle through which a molecule with angluar velocity ω and lifetime τ would rotate before dissociating. Rearranging,

$$\omega\tau = \left[\frac{1 - \beta_{obs}/\beta_{true}}{4(\beta_{obs}/\beta_{true}) - 1} \right]^{1/2}. \tag{8}$$

Thus, to explain a reduction in β from 2.0 to 1.5 ($\beta_{obs}/\beta_{true} = 1.5/2.0$), a rotation of 20° would be required.

The degree to which rotation of excited CF_2BrCH_2I plays a role in reducing the anisotropy can be ascertained from the knowledge of the rotational temperature of the molecule. The rotational temperature in the molecular beam can be estimated by assuming it is equal to the terminal longitudinal translational temperature in the beam, which is related to the α parameter in the form for the velocity distribution (see Section II) by[18]

$$\alpha = \left(\frac{2kT}{m}\right)^{1/2}. \tag{9}$$

For our beam conditions, T is ~35 K, which corresponds to a rotational period of approximately 40 ps for CF_2BrCH_2I. The amount of time required to rotate 20° would be ~2.2 ps—much longer than the expected lifetime of < 400 fs[23,25] of the repulsive state. Given the short lifetime, the excited complex would rotate only a few degrees or less before dissociating, and the anisotropy parameter would change by no more than one percent. Rotation of the excited complex has been observed to reduce the anisotropy in a photofragmentation study[3] of CH_3I, where the sample was near room temperature. Evidently, it is prudent to take advantage of the efficient rotational cooling in a molecular beam in order to render this effect negligible.

The initial tangential velocity component of the dissociating fragment in the excited complex could lead to a resultant fragment velocity oriented along a different direction than the initial C–I bond axis (when the photon was absorbed), thus causing an apparent reduction in the anisotropy parameter. Assuming a fixed rotational (or tangential) velocity, the form for the c.m. angular distribution would be,[19(b)]

$$w(\theta) \propto 1 + \beta_{true} P_2(\cos\gamma) P_2(\cos\theta), \tag{10}$$

where γ is the angle between the initial orientation of the C–I bond and the resultant direction of the fragment velocity. The observed β_{obs} would be the true, or otherwise unperturbed, β reduced by $P_2(\cos\gamma)$. For a CF_2BrCH_2I rotational temperature of 35 K, the tangential velocity of the I fragment would be ~3000 cm/s, and for a typical iodine recoil velocity of 7×10^4 cm/s, the angle γ would be ~2.5°. Consequently, β_{obs} would differ from β_{true} by a fraction of one percent.

Laser saturation of the exctation is another possible reason for an apparently low anisotropy, and its effect has been modeled by Ling and Wilson.[20] Using their model, we derive a slightly more general equation than they reported for the angular distribution,

$$w(\theta) \propto [1 + \beta P_2(\cos\theta)] \int_0^{2\pi} \frac{1 - \exp\{-\sigma F[1 - \frac{\beta}{2} P_2(\sin\theta\cos\chi)]\}}{1 - \frac{\beta}{2} P_2(\sin\theta\cos\chi)} d\chi, \qquad (11)$$

where we see that the simple form of the angular distribution is modified by an integral which cannot be solved analytically. σF is the product of the absorption cross section and the integrated photon flux for the laser pulse. χ is the angle between the angular momentum vector **J** for the rotating parent molecule and the projection of the electric vector **E** onto the plane containing **J**. The fragments seen at the detector do not come from molecules with a single angular momentum orientation, but from molecules with any **J** lying in a plane that is perpendicular to the dissociation coordinate.

This saturation model is really only valid for a diatomic molecule, but CF_2BrCH_2I is sufficiently prolate (the ratio of rotational constants is $A/\overline{B} \approx 11$) that the diatomic model can be used to estimate the effect of saturation. We have incorporated Equation (11) into our data analysis program, and we have concluded that for σF values of ~0.4, for example, the anisotropy parameter, fit without taking into account saturation, would be about 0.2 too low. Nevertheless, as noted previously, only at 248 and 266 nm could saturation effects be important, and they have been

taken into account in the data analysis, so our reported β values should be free from saturation lowering.

It is plausible that the parent molecules could be excited either by a parallel transition to the $^3Q_0$ state or by a perpendicular transition to the ^1Q state. Allowing for curve crossing from either state to the other, then the anisotropy parameter for a particular dissociation channel could fall in between −1.0 and 2.0. The problem with this reasoning is that the experimental results for 266 and 308 nm photodissociation show the same anisotropy for both ground and excited state iodine channels, and it would be highly unlikely that the probability for curve crossing from $^3Q_0$ to ^1Q could be exactly complemented by the probability for curve crossing from ^1Q to $^3Q_0$ such that both channels would have equal β values. Much more reasonable is the explanation that both dissociation channels originate from the same excited state—$^3Q_0$. At 248 nm, the ground state I channel had a slightly lower β than the excited state channel, so it is possible that two excited states could be responsible for dissociation, with the ground state I($^2P_{3/2}$) channel having more perpendicular character than the excited state I($^2P_{1/2}$) channel, but the similarity of the two β values makes this possibility suspect.

A likely explanation for the reduction of β from 2 is distortion of the excited complex before dissociation, which could easily change the direction of fragment recoil with respect to the initial C–I bond axis. This effect is difficult to model quantitatively, but we do have reason to believe it is important. Assuming a rigid radical impulsive model,[1,26] the fraction of the available energy in translation is given by

$$\frac{E_T}{E_{\mathrm{avl}}} = \left[1 + \frac{\mu b^2}{I}\right]^{-1}, \tag{12}$$

where μ is the reduced mass of the two fragments R and I, b is the exit impact parameter, and I is the moment of inertia for the radical R. For CF_2BrCH_2I,

these quantities are 67.5 amu, ~1.5 Å, and 249 amu·Å^2, respectively, where the impact parameter is derived from the equilibrium structure of the molecule. Using these values, the expected fraction of available energy in translation would be 0.62. This fraction should reflect the maximum energy that could appear in translation—assuming no distortion—because a softer radical would channel energy into vibration and reduce this ratio. Table 6 shows that the observed ratios, $E_T(\max)/E_{\mathrm{avl}}$, can be explained for some cases without invoking distortion, while in other cases, they cannot. Most notably, at 308 nm the maximum energy in translation is much higher than expected if the molecule dissociated from its equilibrium configuration. A ratio of 0.73, for example, would require a b of ~1.17, and in order to measure a translational energy equal to the available energy, b would have to be zero. The large deformations which must be occuring at 308 nm probably account for the fact that the β value at 308 nm was the lowest observed.

While the rigid radical model is useful for predicting when distortion must occur, distortion might still occur if the translational energy is less than or equal to that predicted by the model. A deformation of the molecule could result in vibrational excitation of the radical; then the rigid radical picture would not apply. For example, bending of the Br–C–C–I skeleton toward lower exit impact parameter leads to lower rotational excitation and thus greater vibrational excitation, for a given translational energy release. Therefore, even at 248 and 266 nm, where the maximum energy in translation is not much different than the rigid radical prediction, β could be reduced because of bending in the complex. A point not to be overlooked, however, is that the impulsive model should more accurately describe the dissociation process at higher excitation energies (such as 266 and 248 nm), where a steeper part of the dissociative surface is reached. At a lower energy excitation to a more level part of the potential, the C–I bond might not break as fast, allowing

more time for the radical fragment to distort. In addition, bending does not have to happen only in the excited complex. Depending on the wavelength, Franck-Condon factors might favor absorption from a distorted ground state.

The implications of the anisotropy parameter take on meaning insofar as we understand the nature of the electronic transitions involved in the photodissociation process. A quasi-diatomic picture,[7,11,26] which assumes an $n \longrightarrow \sigma^*$ transition localized on the C–I[Br] bond, predicts ground state iodine formation arising from a perpendicular transition to the $^3Q_1$ or ^1Q states, and spin-orbit excited state iodine is predicted to correlate to the $^3Q_0$ state reached by a parallel transition. Within the context of this picture, our observation of ground state I($^2P_{3/2}$) product with a parallel polarization dependence can only be explained by an initial transition to the $^3Q_0$ state and subsequent curve crossing to the ^1Q (or possibly the $^3Q_1$) state.

The quasi-diatomic model is credible because the UV absorption spectrum of CF_2BrCF_2I, for example, resembles closely the sum of the separate CF_3CF_2Br and CF_3CF_2I absorption spectra.[12] In addition, the position and shape of the C–I absorption continuum in CH_3CH_2I is virtually unchanged when a β-hydrogen is substituted with a Cl of Br. Further evidence for localized transitions comes from Butler, *et al.*,[8,9,26] who showed that excitation near the peak of the supposed C–Br absorption continuum in CH_2BrI resulted in simple bond fission of only the stronger C–Br bond. (3-center IBr elimination was also observed, but it was a minor channel.) The demonstration of bond-selective photochemistry helps reinforce our desire to view the C–X chromophores in alkyl halides as local diatomic entities.

Unfortunately, some experimental results exist which must cloud our view. In a photodissociation study of CF_2BrCF_2I,[7] whose aim was bond-selective photochemistry, C–I bond breakage was almost twice as probable as C–Br bond fission even though only the C–Br $n \longrightarrow \sigma^*$ transition should have been pumped. This obser-

vation was rationalized within the quasi-diatomic framework as a local C–Br bond absorption and a high probability for fast resonant electronic energy transfer to the C–I bond. Recent results in our laboratory show that at 308 nm, photodissociation of both CH_2ClCH_2I and CH_2BrCH_2I, yield only ground state iodine product with a *parallel* polarization dependence. It is difficult to imagine that curve crossing could be as efficient as 100 percent. Quite possibly, the assumed $n \longrightarrow \sigma^*$ absorption spectrum of haloethanes (especially *di*haloethanes) is more complicated than our satisfyingly simple diatomic picture, and the transition moment might not be simply parallel (or perpendicular) to the C–X bond. In such a case (see Equation (2)), the anisotropy parameter would be less than 2.

The $I(^2P_{1/2})/I(^2P_{3/2})$ branching ratios reported here can also not be explained under the quasi-diatomic assumption. The large ground state iodine component at 308 nm might be interpreted as arising from a slow velocity through the curve crossing, thereby increasing the curve crossing probability, but this interpretation fails to explain why a greater fraction of $I(^2P_{3/2})$ is observed at 248 nm than at 266 nm. Furthermore, it is well known[7,12,26,27–32] that halogen substitution of hydrogens in alkyl iodides changes the $I(^2P_{1/2})$ quantum yield dramatically. Clearly, a complete understanding of the branching ratios requires consideration of the whole molecule.

B. Thermochemistry

The observation of stable CF_2BrCH_2 radical product in the midst of spontaneous secondary dissociation enables the derivation of the energy threshold for breaking both the C–I and C–Br bonds in CF_2BrCH_2I. The precision in the measured ΔH for Reaction (4) is low because the stable radical peak was too small to allow a careful threshold determination in a manner similar to the previous CH_2ClCH_2I analysis.[6] Other factors, which could affect the accuracy of ΔH, must also be considered.

If initial parent internal energy could not be neglected, then Equation (5) would predict a ΔH that is too low by the amount E^P_{int}. While the rotational energy of the parent CF_2BrCH_2I molecules in the molecular beam is negligible, vibrations are not cooled nearly so well, and the average vibrational energy could be 2.0-2.5 kcal/mole. In photodissociation from a repulsive surface, only a fraction of the vibrational energy (specifically that associated with the C–I bond) can couple to the dissociation coordinate. This fraction should average less than 0.5 kcal/mole. The contribution from internal energy will therefore be small; moreover, at low excitation levels on the order of a few kcal/mole, the vibrational energy distribution must be roughly exponential with a significant fraction in the ground vibrational state, so the observed threshold will arise from molecules with no initial internal excitation.

A potentially more serious inaccuracy in ΔH could result from an exit channel barrier in CF_2BrCH_2 decomposition. The maximum internal energy E^R_{int}(max) at which stable radical can still exist can be found from Equation (5), where the minimum energy in translation E_T(min), derived from the stable CF_2BrCH_2 radical peak, is subtracted from the available energy E^*_{avl}. The presence of a barrier would make E_T(min) too low by an amount equal to the barrier height because decomposition of the CF_2BrCH_2 radicals would only occur above the endoergic limit, where they contain the extra internal energy required to overcome the barrier.

Two barrier types could exist: an intrinsic barrier for the addition of Br to the double bond and a centrifugal barrier generated by the necessity of conserving angular momentum when the product radicals fall apart. The intrinsic barrier should be small or nonexistent (if Br addition to the double bond is similar to Cl addition[33]), but even a small barrier of one or two kcal/mole would be near the uncertainty level of our measurement. The centrifugal barrier could be several kcal/mole for some CF_2BrCH_2 radicals because the exit impact parameter for primary C–I fission

is high (when dissociation occurs from the equilibrium configuration), leaving the radical with a large angular momentum (perhaps as high as $150\hbar$).

The measured E_T(min) will be too low only if the CF_2BrCH_2 radicals, created with internal energies greater than the C–Br bond energy, do not decompose because of a barrier. While an intrinsic barrier cannot be circumvented, it is plausible that, during the long transit time from the interaction region to the ionizer, the radical will distort and stretch to a geometry where the centrifugal barrier might only be 1-2 kcal/mole. Thus, our analysis assumes that nearly all the CF_2BrCH_2 radicals formed with an internal energy above the C–Br endoergicity will dissociate before they can be detected.

A recent photofragmentation study in our laboratory of CF_2BrCF_2I at 266 and 308 nm[34] lends more credence to the unimportance of the centrifugal barrier in the threshold determination. At 266 nm, the low translational energy threshold for existence of stable radical (arising from $I(^2P_{1/2})$ formation) was 13 kcal/mole. At 308 nm, the threshold was observed to be 19.5 kcal/mole when ground state was formed. Analysis of both thresholds produced virtually the *same* value of ΔH for $CF_2BrCF_2I \longrightarrow CF_2CF_2 + Br + I$ (73.3 ± 1 kcal/mole). Given the different translational energies, the angular momenta of the radical fragments should differ by $\sim [E_T(308)/E_T(266)]^{1/2} = 1.23$ in the rigid radical limit ($E_{\rm rot} = L^2/2I_R = E_T\mu b^2/I_R$), and the ratio of barrier heights would be the square of this number, or ~1.5. If a centrifugal barrier were important, we would have expected a higher ΔH from the 308 nm experiment. The CF_2BrCF_2 radical is not an ideal test case, however, because its large size and moment of inertia would result in relatively low levels of rotational excitation—around 3 kcal/mole. And if the centrifugal barrier were to occur at about twice the C–Br bond length, its height would only be ~0.8 kcal/mole, which is within our uncertainty limits. Hence, even though the

CF_2BrCF_2 radical data do not necessarily point to the general unimportance of a centrifugal barrier, such a barrier will be unimportant if the moment of inertia of the radical is large.

The secondary dissociation threshold for CH_2ClCH_2I was also determined at two excitation wavelengths, 248 and 266 nm,[6] and in this case, the two thresholds differed by ~2 kcal/mole. The 248 nm experiment, where the average E_T was greater, yielded the higher value. The chloroethyl radical is substantially smaller than CF_2BrCF_2 and could be formed with as much as 8 kcal/mole in rotation (with dissociation from the equilibrium configuration), which might lead to a centrifugal barrier height of ~2 kcal/mole. The discrepancy between the two experiments was rationalized as experimental error, but the existence of a centrifugal barrier is possibly a better explanation. If a centrifugal barrier were important, even the threshold energy from the 266 nm experiment could be high.

As stated above, any barrier would cause the apparent minimum energy in translation to be too low by an amount equal to the barrier height, making ΔH for Reaction (4) too high by that amount. Because we cannot rule out a barrier entirely, we must ultimately conclude that, rigorously, our result (and any other obtained by the same method) for the reaction enthalpy is an upper limit.

The heat of formation $\Delta H_f^\circ(0)$ of CF_2BrCH_2I follows directly from our result for the ΔH of Reaction (4): $\Delta H_{f,0}^\circ(CF_2BrCH_2I) = -92.6 \pm 2$ kcal/mole (refer to Table 7). The credibility of this result can be confirmed by examining the following scheme:

$$\begin{array}{ccc} CF_3CH_3 & \xrightarrow{60.3} & CF_2BrCH_3 \\ \Big\downarrow{\scriptstyle 23.3} & & \Big\downarrow{\scriptstyle (22.2)} \\ CF_3CH_2I & \xrightarrow[(59.2)]{} & CF_2BrCH_2I \end{array} \qquad (13)$$

The numbers are the changes in $\Delta H_f^\circ(0)$ for each step in units of kcal/mole. Without our experiment result, the values in parentheses would have to be approximated by using the analogous change in $\Delta H_f^\circ(0)$ for the known, less substituted species, in which case the estimated $\Delta H_f^\circ(0)$ of CF_2BrCH_2I would be –91.5 ± 1.5 kcal/mole. Thus, our result is quite reasonable.

If the C-I bond energy of CF_2BrCH_2I were known, then the C–Br bond energy of the CF_2BrCH_2 radical could easily be calculated. Although $D_0^\circ(CF_2BrCH_2\text{–}I)$ is not known exactly, a good assumption would be to set it equal to $D_0^\circ(CF_3CH_2\text{–}I)$ = 55.8 ± 1.7 kcal/mole. Then $D_0^\circ(CH_2CF_2\text{–}Br)$ would equal 67.5–55.8 = 11.7 ± 2.5 kcal/mole. An alternative method of obtaining $D_0^\circ(CH_2CF_2\text{–}Br)$ is to assume that ΔH for $CF_3CH_3 \longrightarrow CF_3CH_2 + H$ is the same as ΔH for $CF_2BrCH_2 \longrightarrow CF_2BrCH_2 + H$. $\Delta H_{f,0}^\circ(CF_2BrCH_2)$ would then equal 61.3 ± 2.0 kcal/mole and the C–Br bond energy in the radical would be 10.6 ± 2.5 kcal/mole. Both estimates are fairly close; nevertheless, a 5 kcal/mole range of uncertainty is unsatisfactory. If either the C–I bond energy of the parent or the R–X radical bond energy were measured for CF_2BrCH_2I and other similar compounds for which ΔH_f° is known, then the thermochemical picture of these iodoethanes would be complete. The effect of substitution in iodoethanes as well as the substitution effect on the bromo(chloro)ethyl radical C–X bond energy would then become clear.

ACKNOWLEDGEMENTS

This work was supported by the Director, Office of Energy Research, Office of Basic Energy Sciences, Chemical Sciences Division of the U.S. Department of Energy under Contract No. DE-AC-0376SF00098. The Nd:YAG laser was on loan from the San Francisco Laser Center, a National Science Foundation Regional Instrumentation Facility, NSF Grant No. CHE79-16250 awarded to the University of

California at Berkeley in collaboration with Stanford University. We would like to thank Dr. Marcos Maestre for allowing us to use his Cary 14 spectrophotometer.

REFERENCES

1. S. Riley and K.R. Wilson, Discuss. Faraday Soc. **53**, 132 (1972).

2. R.K. Sparks, K. Shobatake, L.R. Carlson, and Y.T. Lee, J. Chem. Phys. **75**, 3838 (1981).

3. G.N.A. Van Veen, T. Baller, A.E. De Vries, and N.J.A. Van Veen, Chem. Phys. **87**, 405 (1984).

4. G.N.A. Van Veen, T. Baller, A.E. De Vries, and M. Shapiro, Chem. Phys. **93**, 277 (1985).

5. M.D. Barry and P.A. Gorry, Mol. Phys. **52**, 461 (1984).

6. T.K. Minton, P. Felder, R.J. Brudzynski, and Y.T. Lee, J. Chem. Phys. **81**, 1759 (1984).

7. D. Krajnovich, L.J. Butler, and Y.T. Lee, J. Chem. Phys. **81**, 3031 (1984).

8. L.J. Butler, E.J. Hintsa, S.F. Shane, and Y.T. Lee, J. Chem. Phys., to be published.

9. L.J. Butler, E.J. Hintsa, and Y.T. Lee, J. Chem. Phys. **84**, 4104 (1986).

10. A. Gedanken and M.D. Rowe, Chem. Phys. Lett. **34**, 39 (1975).

11. (a) R.S. Mulliken, Phys. Rev. **50**, 1017 (1936); (b) **51**, 310 (1937); (c) **47**, 413 (1935); (d) J. Chem. Phys. **8**, 382 (1940).

12. W.H. Pence, S.L. Baughcum, and S.R. Leone, J. Phys. Chem. **85**, 3844 (1981).

13. S.J. Lee, and R. Bersohn, J. Phys. Chem. **86**, 728 (1982).

14. A.M. Wodtke and Y.T. Lee, J. Phys. Chem. **89**, 4744 (1985).

15. P.S. Weiss, Ph.D. thesis, University of California, Berkeley, 1986.

16. M. Vernon, "KELVIN Rare Gas Time-of-Flight Program," Lawrence Berkeley Laboratory Report No. 12422, 1981.

17. D.J. Krajnovich, Ph.D. thesis, University of California, Berkeley, 1983.

18. R.B. Berstein, *Chemical Dynamics via Molecular Beam and Laser Techniques* (Oxford University, New York, 1982), p. 30.

19. (a) G.E. Busch and K.R. Wilson, J. Chem. Phys. **56**, 3626 (1972); (b) **56**, 3638 (1972).

20. J.H. Ling and K.R. Wilson, J. Chem. Phys. **65**, 881 (1976).

21. C. Jonah, J. Chem. Phys. **55**, 1915 (1971).

22. D. Porret and C.F. Goodeve, Proc. R. Soc. London Ser. A **165**, 31 (1938).

23. M. Dzvonik, S. Yang, and R. Bersohn, J. Chem. Phys. **61**, 4408 (1974).

24. (a) J.V.V. Kasper, J.H. Parker, and G.C. Pimentel, J. Chem. Phys. **43**, 1827 (1965); (b) M.A. Pollack, Appl. Phys. Lett. **8**, 36 (1966).

25. A. Zewail (private communication).

26. L.J. Butler, Ph.D. thesis, University of California, Berkeley, 1985.

27. C.A. Wight and S.R. Leone, J. Phys. Chem. **87**, 5299 (1983).

28. T. Donohue and J.R. Wiesenfeld, J. Chem. Phys. **63**, 3130 (1975).

29. W.L. Ebstein, J.R. Wiesenfeld, and G.L. Wolk, Chem. Phys. Lett. **53**, 185 (1978).

30. J.B. Koffend and S.R. Leone, Chem. Phys. Lett. **81**, 136 (1981).

31. J.E. Smedley and S.R. Leone, J. Chem. Phys. **79**, 2687 (1983).

32. E. Gerck, J. Chem. Phys. **79**, 311 (1983).

33. H. B. Schlegel and C. Sosa, J. Phys. Chem. **88**, 1141 (1984).

34. T.K. Minton, G.M. Nathanson, S.F. Shane, and Y.T. Lee, to be submitted to J. Chem. Phys.

35. *JANAF Thermochemical Tables*, 2nd ed. Natl. Stand. Ref. Data Ser., U.S. Natl. Bur. Stand **37** (U.S. GPO, Washington, D.C., 1971).

36. J.D. Cox and G. Pilcher, *Thermochemistry of Organic and Organometallic Compounds*, Academic Press, New York, N.Y., 1970.

37. J.C. Traeger and R.G. McLoughlin, J. Am. Chem. Soc. **103**, 3647 (1981).

38. A.L. Castelhano, P.R. Marriott, and D. Griller, J. Am. Chem. Soc. **103**, 4262 (1981).

39. S.W. Benson and A. Amano, J. Chem. Phys. **36**, 3464 (1962).

40. A.S. Rodgers and W.G.F. Ford, Int. J. Chem. Kinet. **5**, 965 (1973).

41. J.M. Pickard and A.S. Rodgers, Int. J. Chem. Kinet. **9**, 759 (1977).

42. S.S. Chen, A.S. Rodgers, J. Chao, R.C. Wilhoit, and B.J. Zwolinski, J. Phys. Chem. Ref. Data **4**, 441 (1975).

43. G.S. Buckley, W.G.F. Ford, and A.S. Rodgers, Thermochim. Acta **42**, 349 (1980).

44. E.C. Wu and A.S. Rodgers, J. Phys. Chem. **78**, 2315 (1974).

45. S.S. Chen, A.S. Rodgers, J. Chao, R.C. Wilhoit, and B,J, Zwolinski, Natl. Stand. Ref. Data Ser., Natl. Bur. Stand. **No. 3-35706** (Jan. 1974).

46. G.S. Buckley, W.G.F. Ford, and A.S. Rodgers, Thermochim. Acta **49**, 199 (1981).

47. E.C. Wu, J.M. Pickard, and A.S. Rodgers, J. Phys. Chem. **79**, 1078 (1975).

48. T.K. Minton, G.M. Nathanson, S.F. Shane, and Y.T. Lee, to be submitted to J. Chem. Phys.

49. J.M. Pickard and A.S. Rodgers, J. Am. Chem. Soc. **99**, 691 (1977).

50. E.C. Wu and A.S. Rodgers, J. Am. Chem. Soc. **98**, 6112 (1976).

51. S.W. Benson, J. Chem. Ed. **42**, 502 (1965).

TABLE I. Parameters obtained by fitting measured beam number density distributions to the form: $N(v) \propto v_2 \exp[-(v/\alpha - S)^2]$. The peak (most probable) velocity is given by $v_{PK} = \frac{1}{2}\alpha S[1 + \sqrt{1 + 4/S^2}]$. α and v_{PK} are in units of cm/sec.

	Calibration		
Wavelength	α	S	v_{PK}
266 nm	4272[a]	16.87[a]	72,320[a]
	4829[b]	14.43[b]	70,020[b]
248 nm	5039	13.93	70,550
308 nm	4998	13.96	70,130

[a] I^+ TOF data
[b] all other TOF data at 266 nm

TABLE II. Absorption cross section σ and product of cross section and laser intensity F for the three wavelengths studied. Estimated errors in the two quantities are $\pm 10\%$ and $\pm 20\%$, respectively.

		σF	
Wavelength	$\sigma(\times 10^{-19}\ \mathrm{cm}^2)$	Horizontal polarization	Vertical polarization
248 nm	3.2	0.27	0.45
266 nm	5.2	0.42	0.42
308 nm	0.32	0.057	0.087

TABLE III. Observed and calculated horizontal/vertical polarization signal ratios for 266 nm photodissociation at a source angle of 20°.

trial β	Horizontal/Vertical	
—	4.11	observed
1.5	3.73	
1.6	4.05	best
1.7	4.43	

TABLE IV. Observed and calculated horizontal/vertical polarization signal ratios for 248 nm photodissociation at a source angle of 20°. β^* refers to the $I(^2P_{1/2})$ component and β refers to the $I(^2P_{3/2})$ component.

trial β (β^*, β)	Horizontal/Vertical	
———	4.50	observed
1.3, 0.95	3.38	
1.5, 1.15	4.11	
1.6, 1.25	4.54	best
1.7, 1.35	5.03	

TABLE V. Observed and calculated horizontal/vertical polarization signal ratios for 308 nm photodissociation at a source angle of 20°.

trial β	Horizontal/Vertical	
—	3.00	observed
1.0	2.56	
1.1	2.79	
1.2	3.04	best
1.3	3.32	
1.4	3.63	

TABLE VI. Fraction of available energy in translation for each iodine dissociation channel [I($^2P_{3/2}$) and I*($^2P_{1/2}$)] for the minimum, maximum, and average translational energy in each $P(E_T)$.

	E_T/E_{avl}			E_T^*/E_{avl}^*		
Wavelength	E_T(min)	E_T(max)	$< E_T >$	E_T^*(min)	E_T^*(max)	$< E_T^* >$
248 nm	0.28	0.59	0.41	0.15	0.61	0.41
266 nm	0.35	0.58	0.45	0.17	0.73	0.46
308 nm	0.27	0.73	0.51	0.13	1.0	0.65

TABLE VII. Standard molar enthalpies of formation for some substances at 300 K and 0 K.

Species	ΔH_f°(300 K) (kcal/mole)	ΔH_f°(0 K) (kcal/mole)	Reference
H	52.103±0.001	51.631±0.001	35
F	18.86±0.40	18.36±0.40	35
Br	26.74±0.07	28.19±0.07	35
I	25.53±0.01	25.63±0.01	35
$CH_2{=}CH_2$	12.53±0.07	14.58±0.07	35
$CF_2{=}CH_2$	−80.5±1.0	−78.9±1.2[a]	36
$CF_2{=}CF_2$	−157.4±0.7	−156.6±0.7	35
CH_3CH_3	−20.08±0.05	−16.33±0.05[a]	37
CH_3CH_2Br	−15.2±0.5	−10.0±0.5	36
CH_3CH_2I	−2.0±0.4	1.90±0.5[a]	38
CH_2ICH_2I	15.9±0.2	19.7±0.3[a]	39
CH_3CF_3	−178.2±0.4	−175.1±0.6[a]	40
CH_3CF_2Br	−114.2±1.5	−109.3±1.5[a]	41
CH_3CF_2I	−98.9±1.5	−95.9±1.6[a]	42
CF_3CH_2Br	−166.0±0.5	−161.6±0.7[a]	43
CF_3CH_2I	−154.3±0.7	−151.8±1.0[a]	44
CF_2BrCH_2I	−96.9±2.0[a]	−92.6±2.0	this work
CF_3CF_3	−320.9±0.8	−318.9±0.8[a]	45
CF_3CF_2Br	−254.4±1.0	−251.0±1.0[a]	46
CF_3CF_2I	−240.0±1.0	−238.0±1.0[a]	47
CF_2BrCF_2I	−179.5±1.0[a]	−176.1±1.0	48
CF_2ICF_2I	−167.4±1.0[a]	−165.4±1.0	48
$CH_3CH_2\cdot$	28.0±1.0	30.6±1.0[a]	38
$CH_3CF_2\cdot$	−72.3±1.8	−70.0±2.0[a]	49
$CF_3CH_2\cdot$	−123.6±1.2	−121.6±1.4[a]	44
$CF_3CF_2\cdot$	−213.0±1.3	−211.6±1.3[a]	50

[a]Calculated by correcting for thermal energy (Ref. 51)

FIGURE CAPTIONS

Figure 1. Rotating molecular beam source photofragmentation apparatus. 1. Nozzle assembly; 2. Nozzle heating; 3. Cryostatic collimation slit; 4. Laser focussing lens; 5. Laser/molecular beam crossing point; 6. LN cooled panels; 7. Dectector gate valve; 8. Retractable chopping wheel; 9. Main chamber diffusion pump; 10. Source chamber diffusion pump; 11. Electron-impact ionizer; 12. Q-pole mass spectrometer; 13. Magnetically suspended turbopump; 14. Exit ion optics; 15. Ion target; 16. Scintillator; 17. Detector grease-sealed turbopumps; 18. Photomultiplier tube; 19. LN Dewars. The time-of-flight (TOF) spectra of the photoproducts are measured by firing a pulsed ArF laser at point 5 and measuring the time required for the signal at a defined m/e to appear at the detector, 11. The calibrated flight length allows the determination of the lab-frame velocity. By vectorially subtracting the parent beam velocity, measured with the retractable chopping wheel at 8, the center-of-mass (c.m.) velocity distributions of the photoproducts are obtained.

Figure 2. UV absorption spectrum of gaseous CF_2BrCH_2I measured with a Cary 14 spectrophotometer. The broad absorption peak centered at 263 nm is attributed to excitation of a nonbonding 5pπ iodine electron to a σ^* molecular orbital localized on the C–I bond. An analogous absorption also exists for the C–Br chromophore and occurs at shorter wavelengths. In this figure, the low energy tail of the C–Br absorption is observed.

Figure 3. Laboratory TOF distributions of I atom product at 266 nm (horizontal laser polarization) for five source angles. o Experimental points; —— overall fit calculated using the total $P(E_T)$ distribution in Fig. 15 and $\beta = 1.6$; - - - - calculated

fits using the component $P(E_T)$'s in Fig. 15.

Figure 4. Laboratory angular distribution of I atom product at 266 nm (horizontal polarization). ● Experimental points obtained by integrating and normalizing the TOF distributions in Fig. 3. $\pm 2\sigma$ error bars (statistical counting error) are smaller that the symbols. —— $\beta = 1.5$; - - - - $\beta = 2.0$.

Figure 5. Kinematic diagram showing the relationship between the molecular beam velocity $\mathbf{v}_b$, the center-of-mass recoil velocity $\mathbf{v}_{cm}$, and the laboratory velocity flux distribution, I(v). The laboratory (source) angle Θ, and the c.m. angles, $\theta_{\parallel}$ and $\theta_{\perp}$, are also shown. The c.m. angle θ is the angle between the electric vector of the laser light and the c.m. recoil direction of the products. $\theta_{\parallel}$ is the c.m. angle when the laser is polarized parallel (horizontal polarization) to the detector axis, and $\theta_{\perp}$ is the c.m. angle when the laser is polarized perpendicular (vertical polarization) to the detector axis. θ(min) refers to the minimum c.m. angle in the range of the I(v) distribution. The curves depicting the ratios, $\cos^2\theta/\cos^2[\theta(\text{min})]$, show that $\cos^2\theta_{\perp}$ changes almost a factor of 5 more than $\cos^2\theta_{\parallel}$ over the range of I(v). Thus, when the transition moment is approximately parallel to the C–I bond (i.e., $w(\theta) \sim \cos^2\theta$), the fits to the data will be much more sensitive to the angular distribution when the laser polarization is vertical rather than horizontal.

Figure 6. Laboratory TOF distribution of I atom product with vertical laser polarization at 266 nm and a source angle of 20°. The calculated fits all use the same $P(E_T)$ distribution (Fig. 15) but different β parameters in order to illustrate the sensitivity of the fit to β.

Figure 7. (a) Laboratory TOF distribution of products detected at $m/e = 79$

at 266 nm (horizontal polarization) for $\Theta = 20°$. Only the experimental points are shown. The arrow points to a small peak resulting from stable CF_2BrCH_2 radical product which is detected at the bromine mass. The sharp fast feature is mostly due to primary C–Br bond fission, with some of the fastest signal coming from secondary *photo*dissociation. The broad background arises from spontaneous secondary dissociation of the internally excited CF_2BrCH_2 primary product. (b) Blow-up of (a) in the region of the stable radical peak with the calculated TOF of the CF_2BrCH_2 fragment if it had all been stable (and able to be detected at $m/e = 79$). As expected, the stable radical peak corresponds in arrival time to the fast edge of the calculated excited state $I(^2P_{1/2})$ TOF.

Figure 8. Laboratory TOF distribution of products detected at $m/e = 64$ at 266 nm (horizontal polarization) for $\Theta = 20°$. The sharp fast peak arises from secondary photodissociation, while the broad background comes from spontaneous secondary dissociation of the internally hot radical photofragment. The arrow at 300 μs marks the expected arrival time of the stable CF_2BrCH_2 radical product based on its position in the $m/e = 79$ TOF.

Figure 9. Laboratory TOF distributions of I atom product at 248 nm (horizontal polarization) for four source angles. o Experimental points; ——overall fit calculated using the total $P(E_T)$ distribution in Fig. 15 with $\beta = 1.25$ for the $I(^2P_{3/2})$ channel and $\beta = 1.6$ for the $I(^2P_{1/2})$ channel. - - - - calculated fits using the component $P(E_T)$'s in Fig. 15 with their respective β parameters.

Figure 10. Laboratory TOF distribution of I atom product with vertical laser polarization at 248 nm and a source angle of 20°; ——, - - - - calculated fits from the total and component $P(E_T)$ distributions , respectively, in Fig. 15. $\beta = 1.25$

for the faster $I(^2P_{3/2})$ channel and $\beta = 1.6$ for the slower $I(^2P_{1/2})$ channel.

Figure 11. Laboratory TOF distribution of products detected at $m/e = 79$, $\Theta = 20°$, and λ =248 nm for both horizontal and vertical laser polarizations. Only the experimental points are shown. The horizontal polarization TOF is qualitatively similar to that at 266 nm (see Fig. 7).

Figure 12. Laboratory TOF distribution of products detected at $m/e = 64$ at 248 nm (horizontal polarization) for $\Theta = 20°$. Only the experimental points are shown. The most prominent peak, occurring at ~300μs, is contamination in the TOF from $m/e = 63.5$ (I^{++}). The smaller, faster peak comes from secondary photodissociation (see Fig. 8). The broad background is, as usual, the result of spontaneous secondary dissociation.

Figure 13. Laboratory TOF distributions of I atom product at 308 nm (horizontal polarization) for four source angles. o Experimental points; —— overall fit calculated using the total $P(E_T)$ distribution in Fig. 15 and $\beta = 1.2$; - - - - calculated fits using the component $P(E_T)$'s in Fig. 15.

Figure 14. Laboratory TOF distribution of products detected at $m/e = 79$ at 308 nm (horizontal polarization) for $\Theta = 20°$. The experimental points are shown along with a calculated TOF, which assumes that all the CF_2BrCH_2 photoproduct is stable and detectable at $m/e = 79$.

Figure 15. Center-of-mass recoil translational energy distributions for CF_2BrCH_2I photodissociation at 248, 266, and 308 nm. The *solid* curve shows the total $P(E_T)$ derived from fitting the time-of-flight data of the iodine fragment. The *dashed* curves depict the estimated deconvolution of the total $P(E_T)$ into the distributions for each

of the two possible dissociation channels. The relative probability of each channel is shown under the product iodine state. The low energy shoulder in the 248 and 266 nm $P(E_T)$'s is a result of I atom detection following primary C–Br bond fission (see text); thus, the shoulder is not part of the photodissociation process represented here, and the curve for the excited state iodine channel has been smoothly extended such that is does not include the shoulder.

Figure 16. Energy level diagram for photodissociation of CF_2BrCH_2I at 248, 266, and 308 nm. The total $P(E_T)$ distributions are shown in order to illustrate the relationship between the translational energy distributions and the energy available for translation. The asterisk (*) refers to the spin-orbit excited state $^2P_{1/2}$ of the atom.

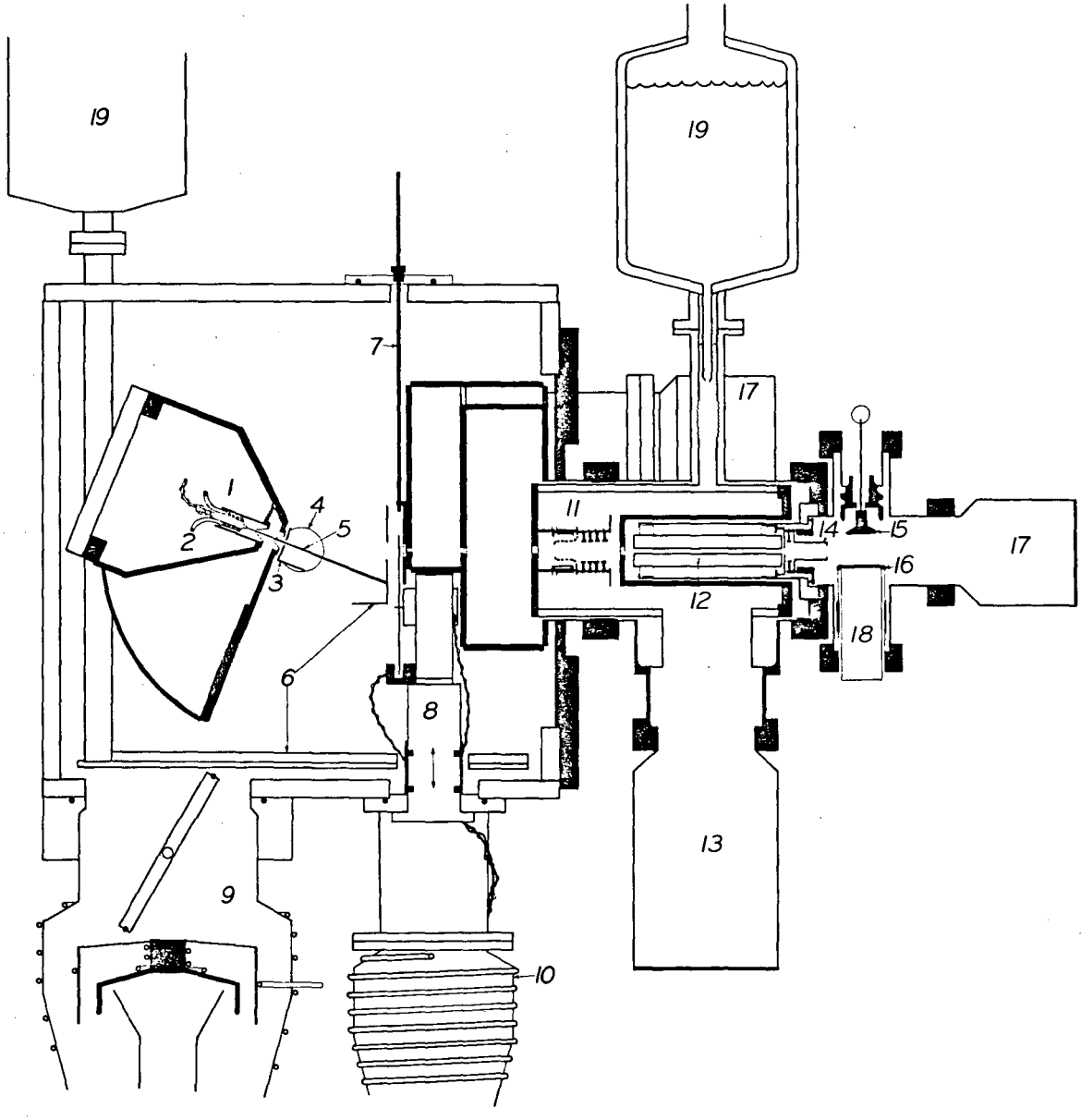

XBL 862-713

Figure 1

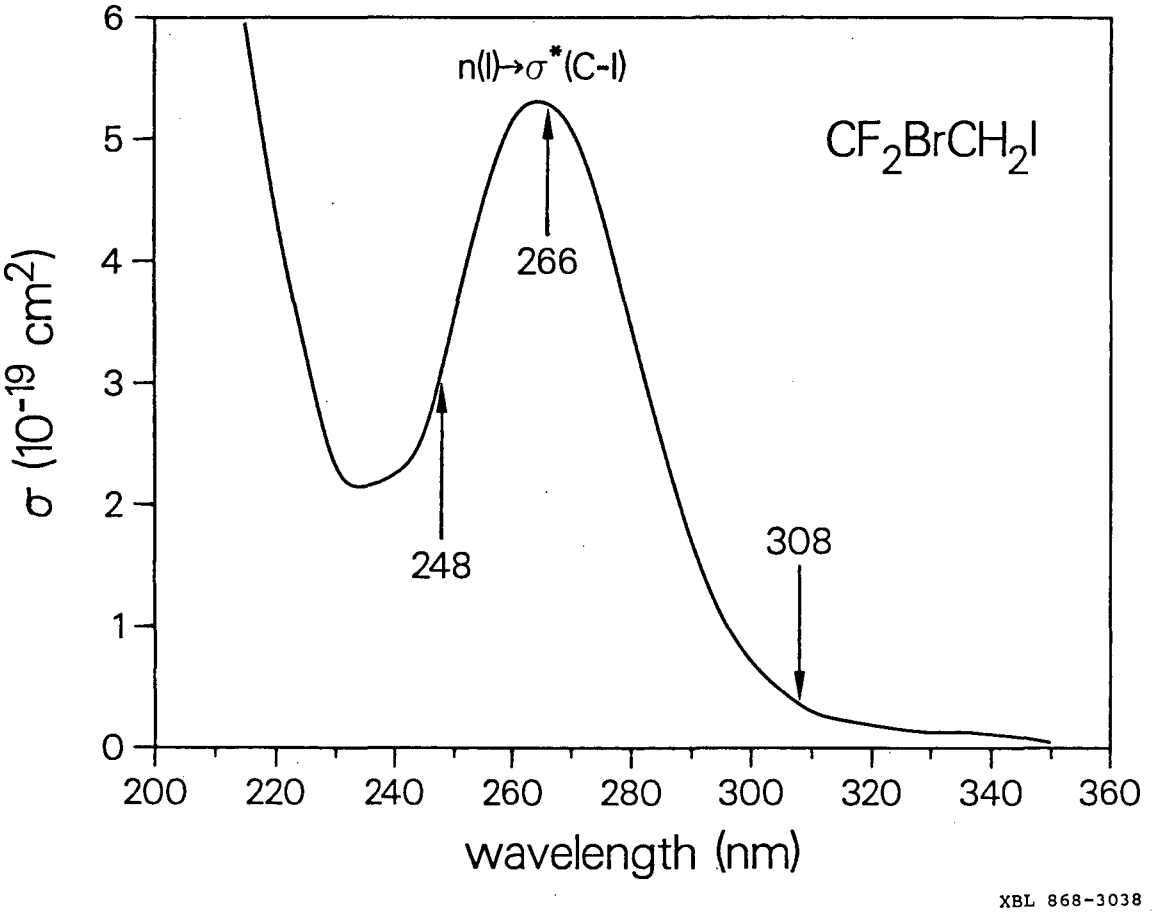
n(I)→σ*(C-I)
CF2BrCH2I
266
248
308
σ (10-19 cm2)
wavelength (nm)
0
1
2
3
4
5
6
200
220
240
260
280
300
320
340
360
XBL 868-3038

Figure 2

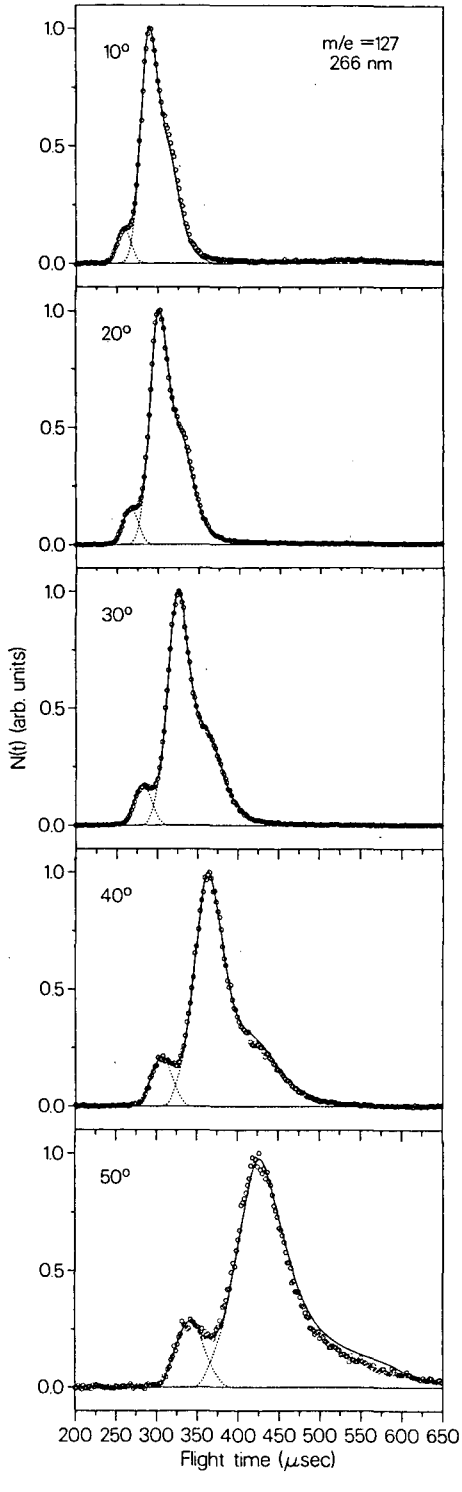

XBL 867-2707

Figure 3

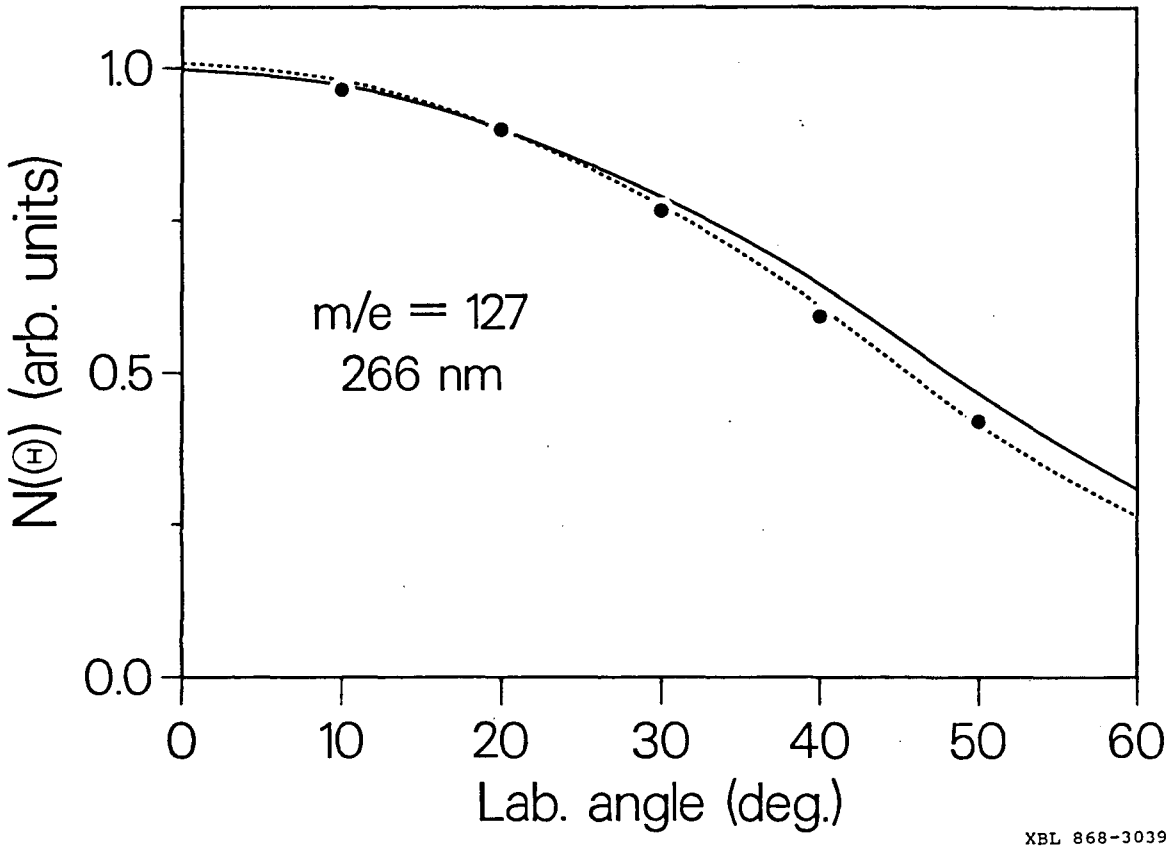
1.0
0.5
0.0
N(Θ) (arb. units)
m/e = 127
266 nm
0
10
20
30
40
50
60
Lab. angle (deg.)
XBL 868-3039

Figure 4

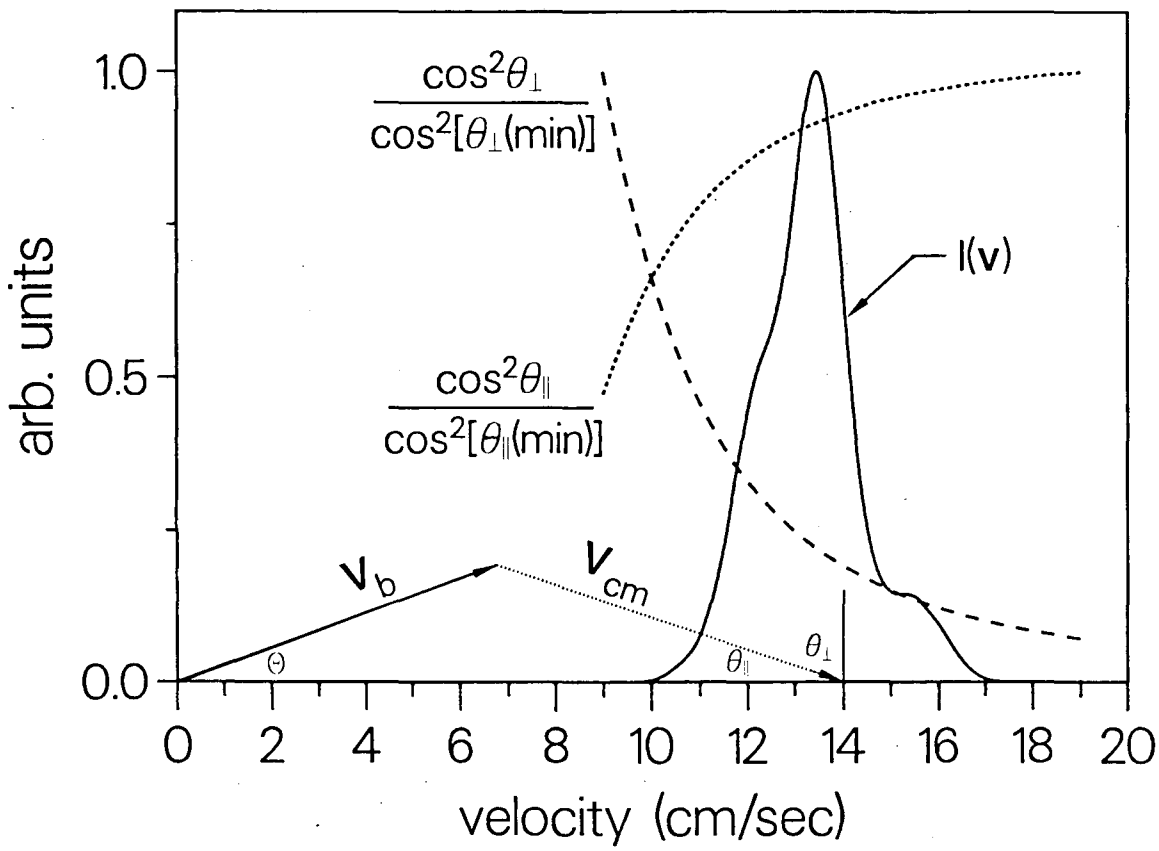

XBL 868-3037

Figure 5

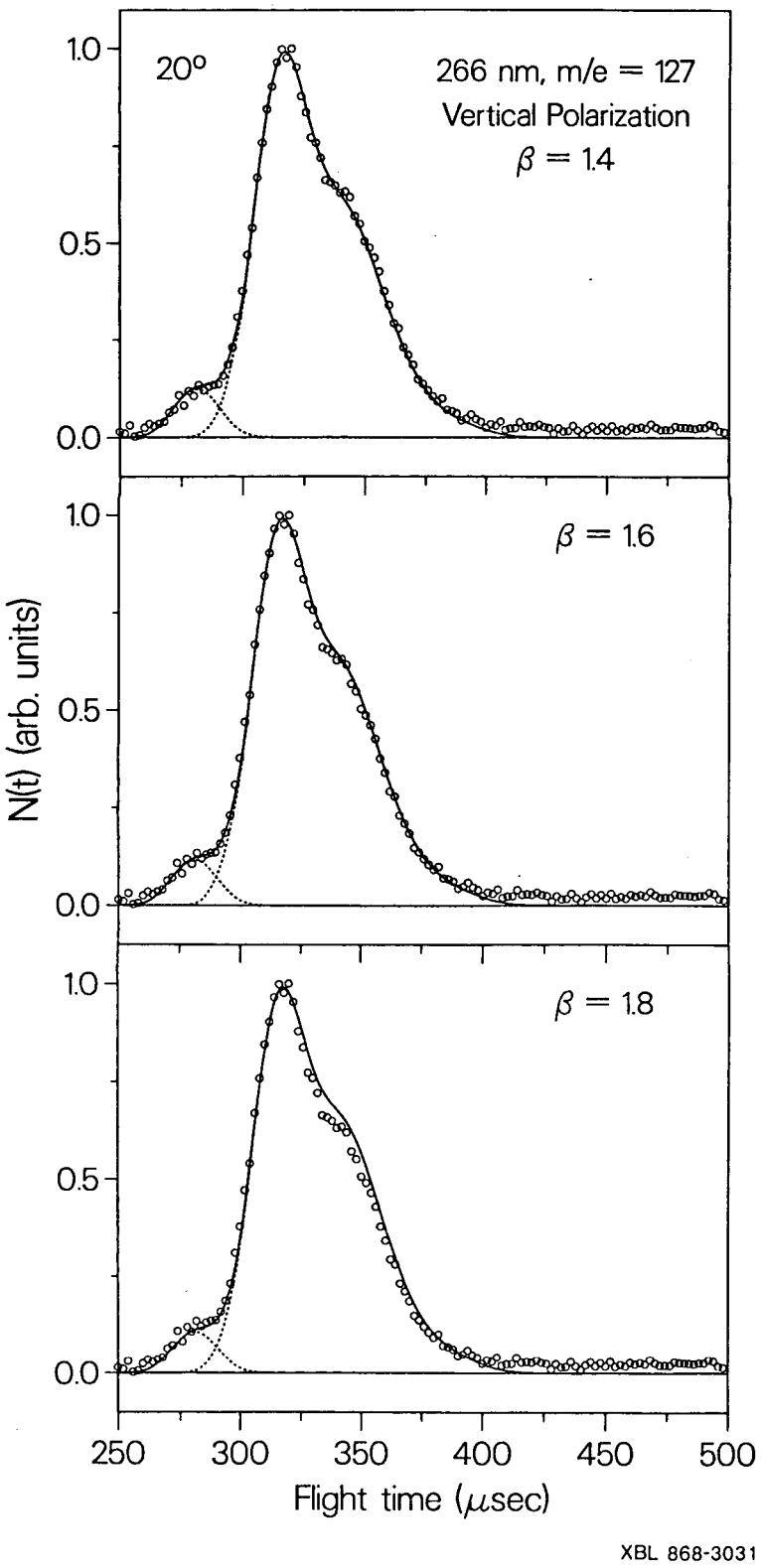
20°
266 nm, m/e = 127
Vertical Polarization
β = 1.4
β = 1.6
β = 1.8
1.0
0.5
0.0
N(t) (arb. units)
250
300
350
400
450
500
Flight time (μsec)
XBL 868-3031

Figure 6

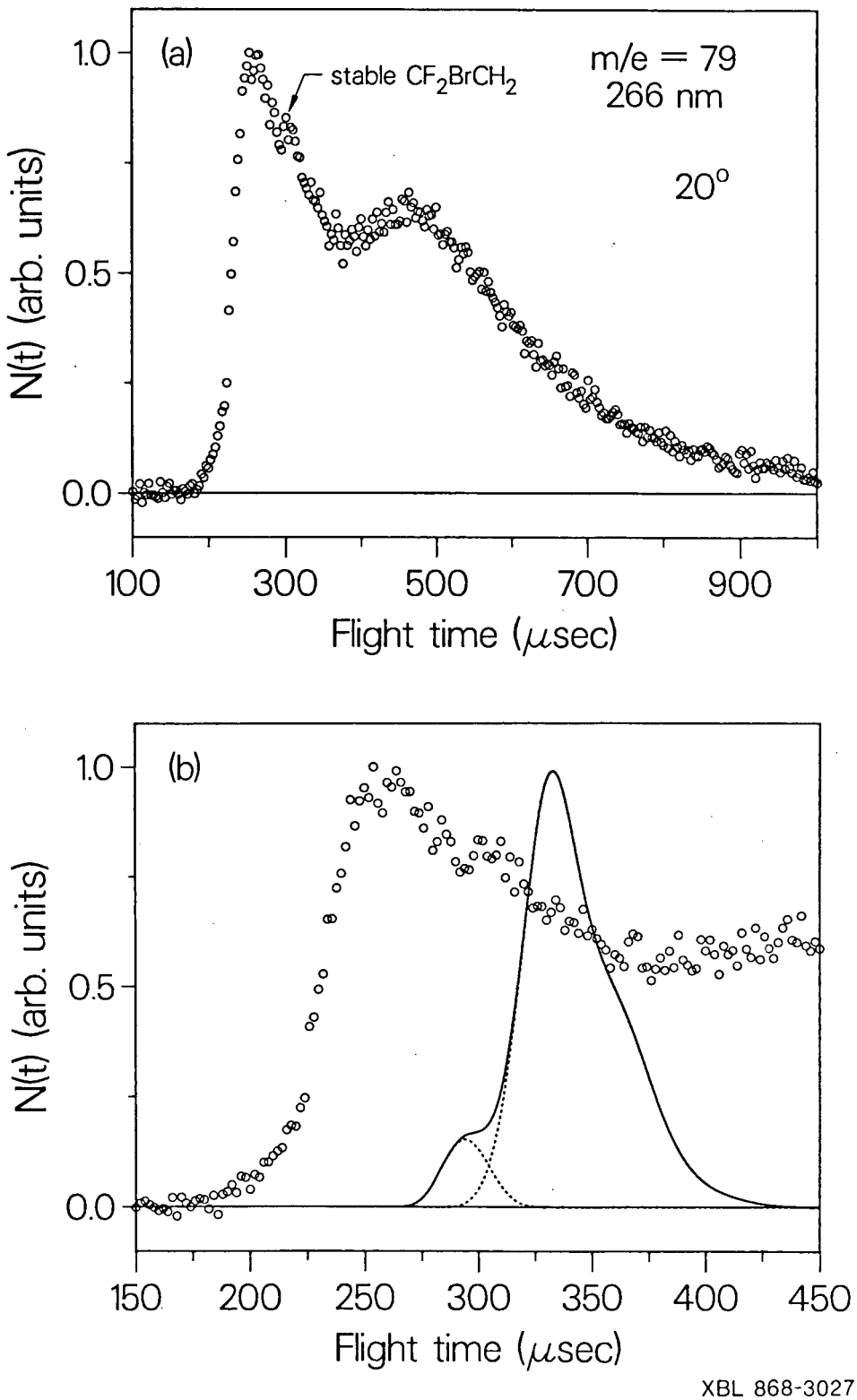
(a)
stable CF_2BrCH_2
m/e = 79
266 nm
20°
1.0
0.5
0.0
N(t) (arb. units)
100
300
500
700
900
Flight time (μsec)
(b)
1.0
0.5
0.0
N(t) (arb. units)
150
200
250
300
350
400
450
Flight time (μsec)
XBL 868-3027

Figure 7

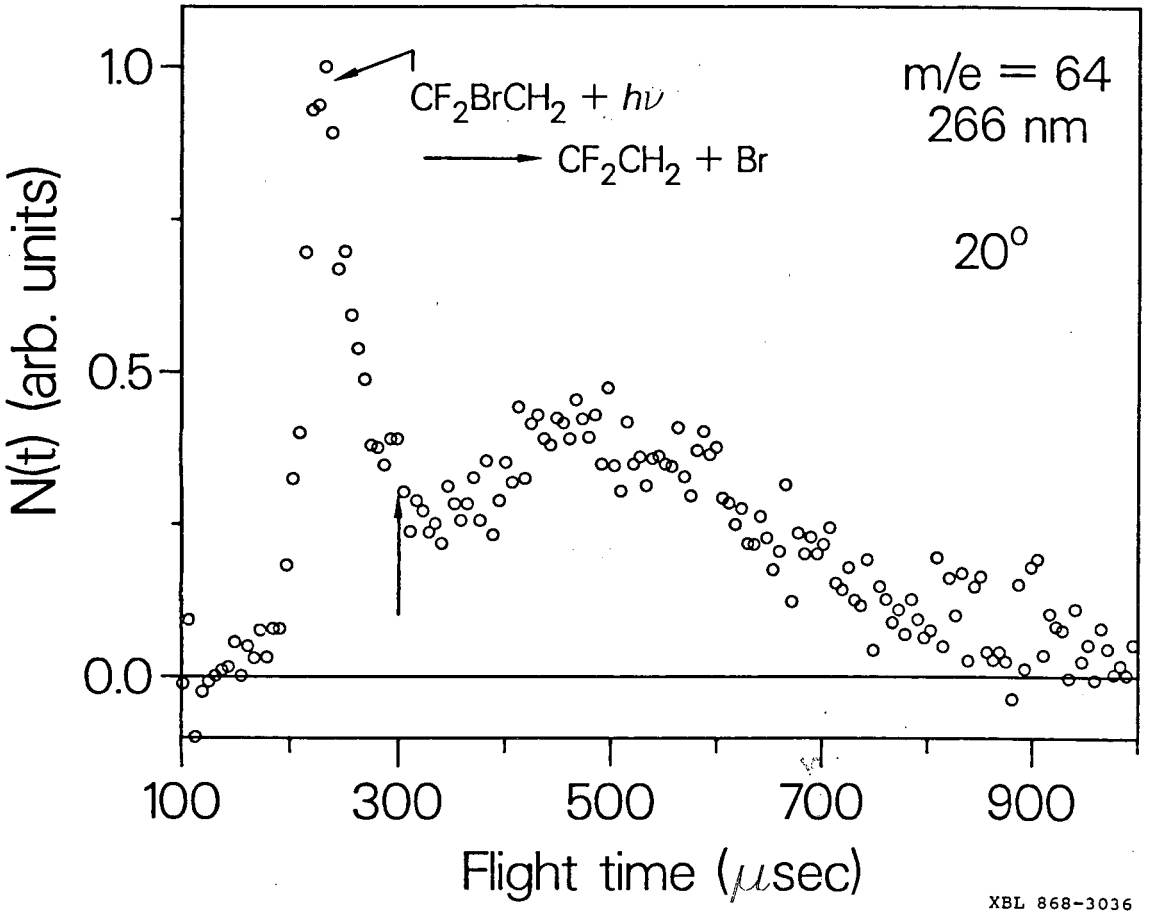
1.0
0.5
0.0
N(t) (arb. units)
$CF_2BrCH_2 + h\nu$
$\longrightarrow CF_2CH_2 + Br$
m/e = 64
266 nm
20°
100
300
500
700
900
Flight time (μsec)
XBL 868-3036

Figure 8

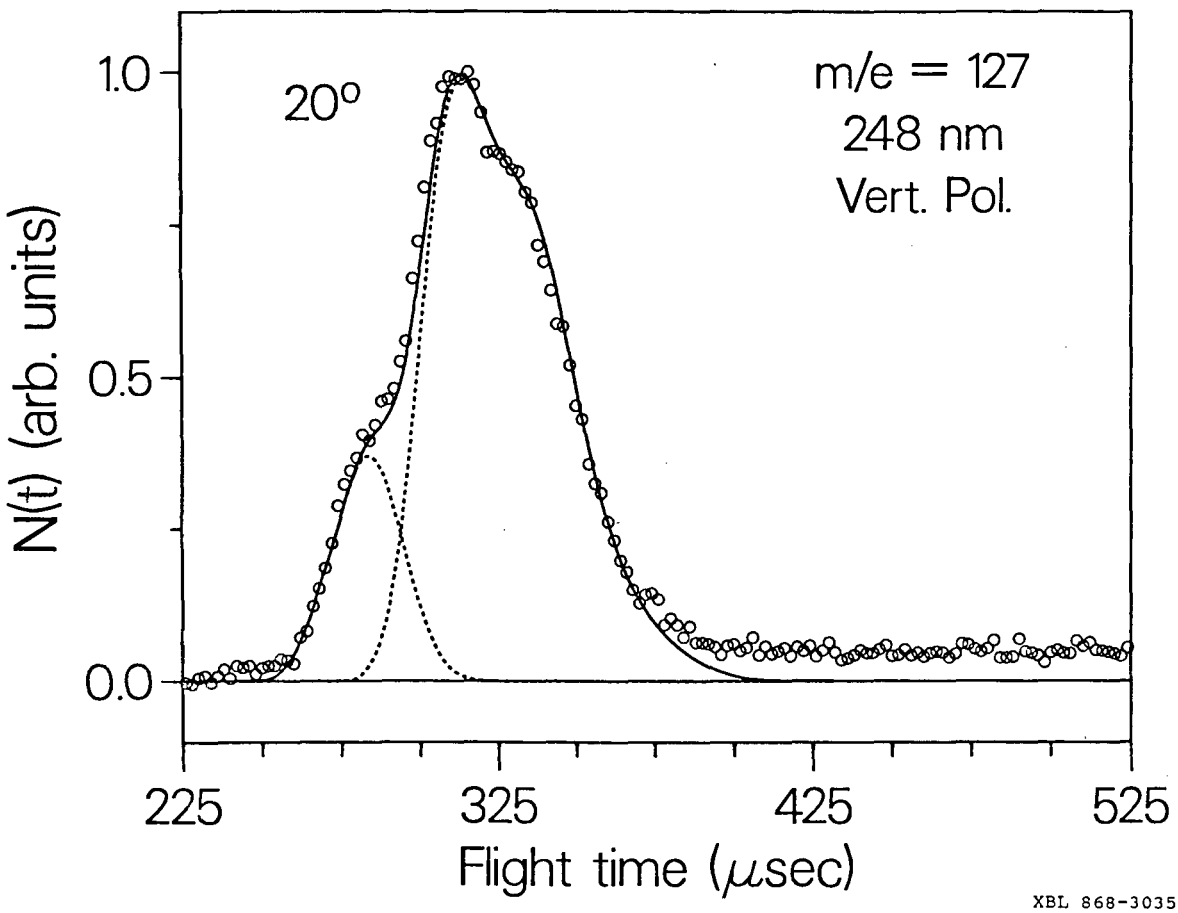
1.0
0.5
0.0
N(t) (arb. units)
20°
m/e = 127
248 nm
Vert. Pol.
225
325
425
525
Flight time (μsec)
XBL 868-3035

Figure 9

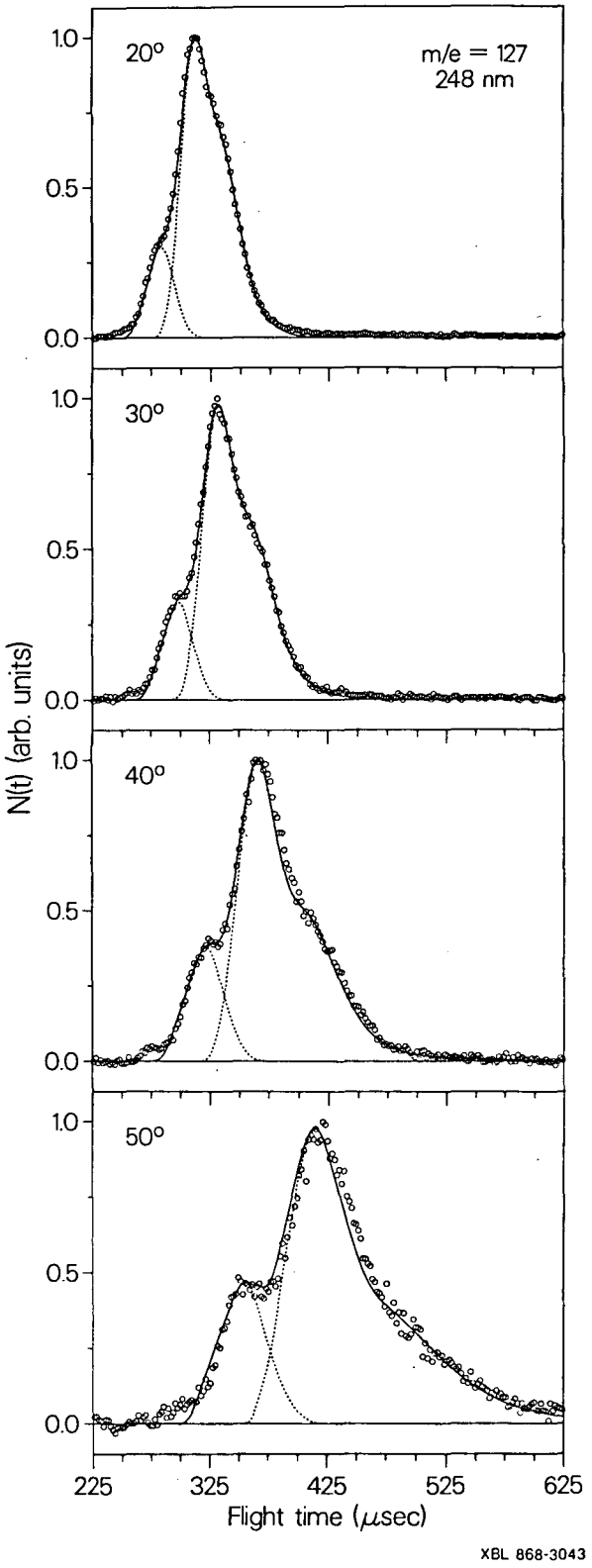
20°
m/e = 127
248 nm
30°
40°
50°
1.0
0.5
0.0
N(t) (arb. units)
225
325
425
525
625
Flight time (μsec)
XBL 868-3043

Figure 10

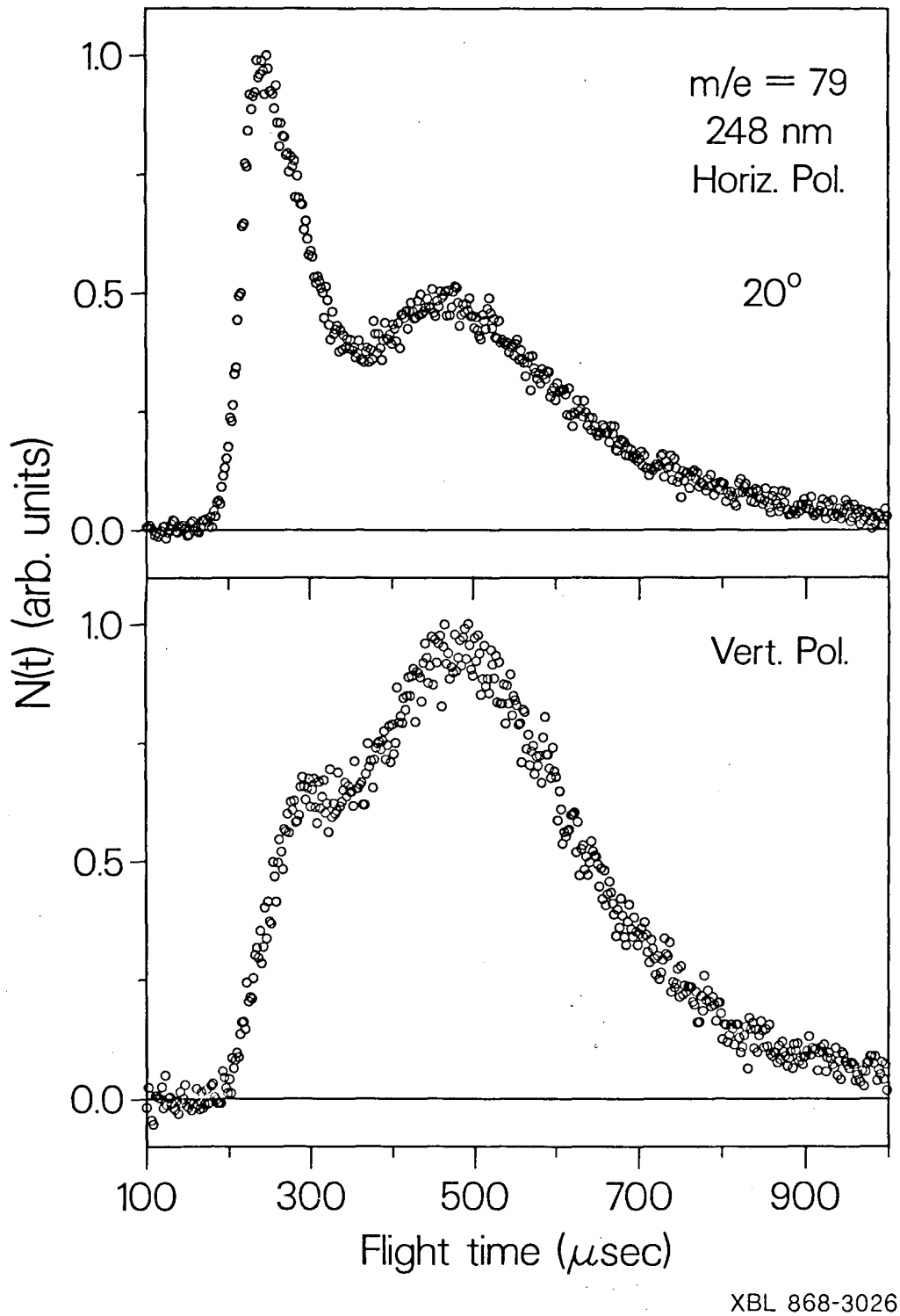
m/e = 79
248 nm
Horiz. Pol.
20°
Vert. Pol.
1.0
0.5
0.0
N(t) (arb. units)
100
300
500
700
900
Flight time (μsec)
XBL 868-3026

Figure 11

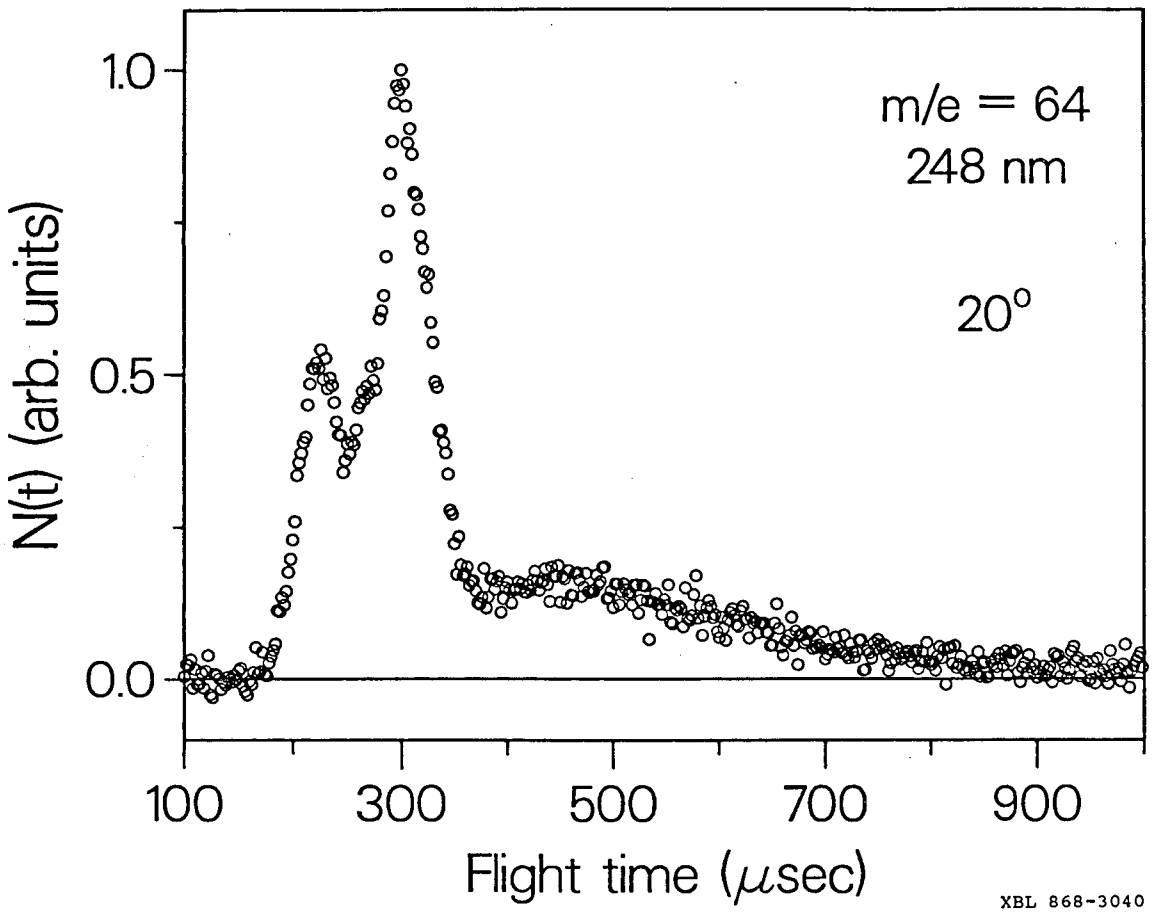
1.0
0.5
0.0
N(t) (arb. units)
m/e = 64
248 nm
20°
100
300
500
700
900
Flight time (μsec)
XBL 868-3040

Figure 12

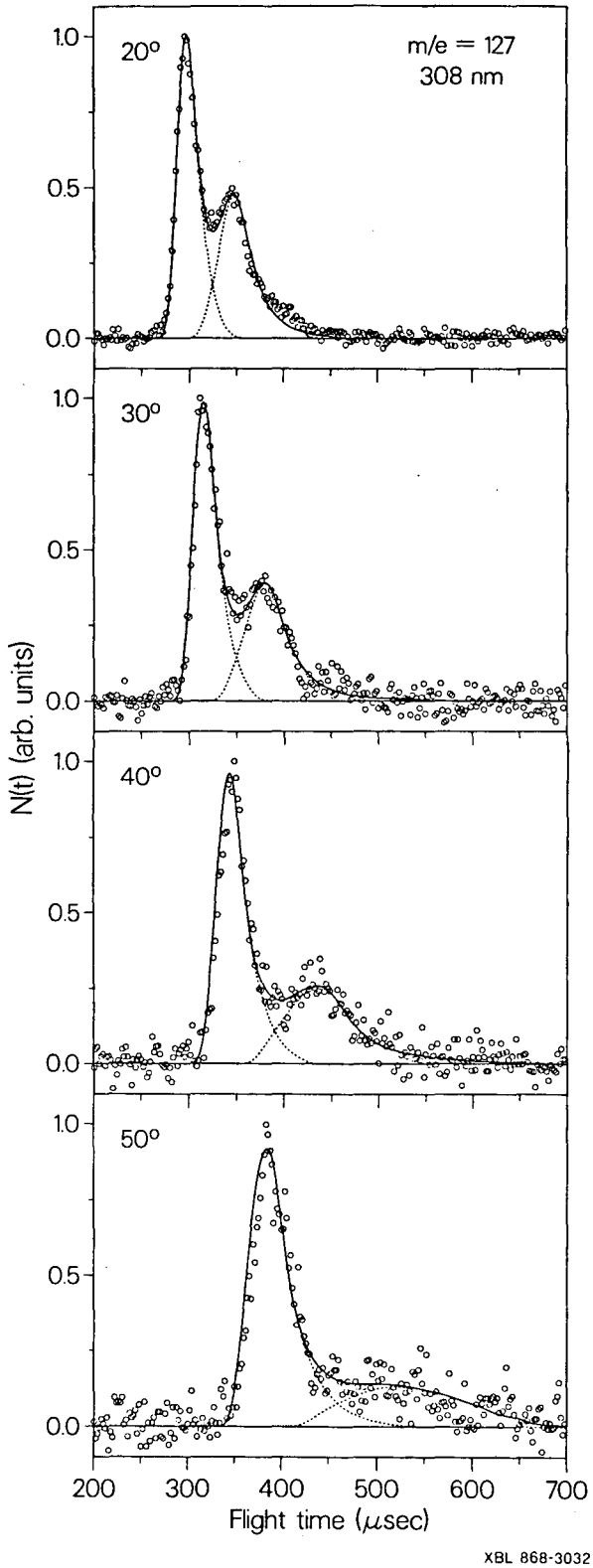
m/e = 127
308 nm
20°
30°
40°
50°
1.0
0.5
0.0
N(t) (arb. units)
200
300
400
500
600
700
Flight time (μsec)
XBL 868-3032

Figure 13

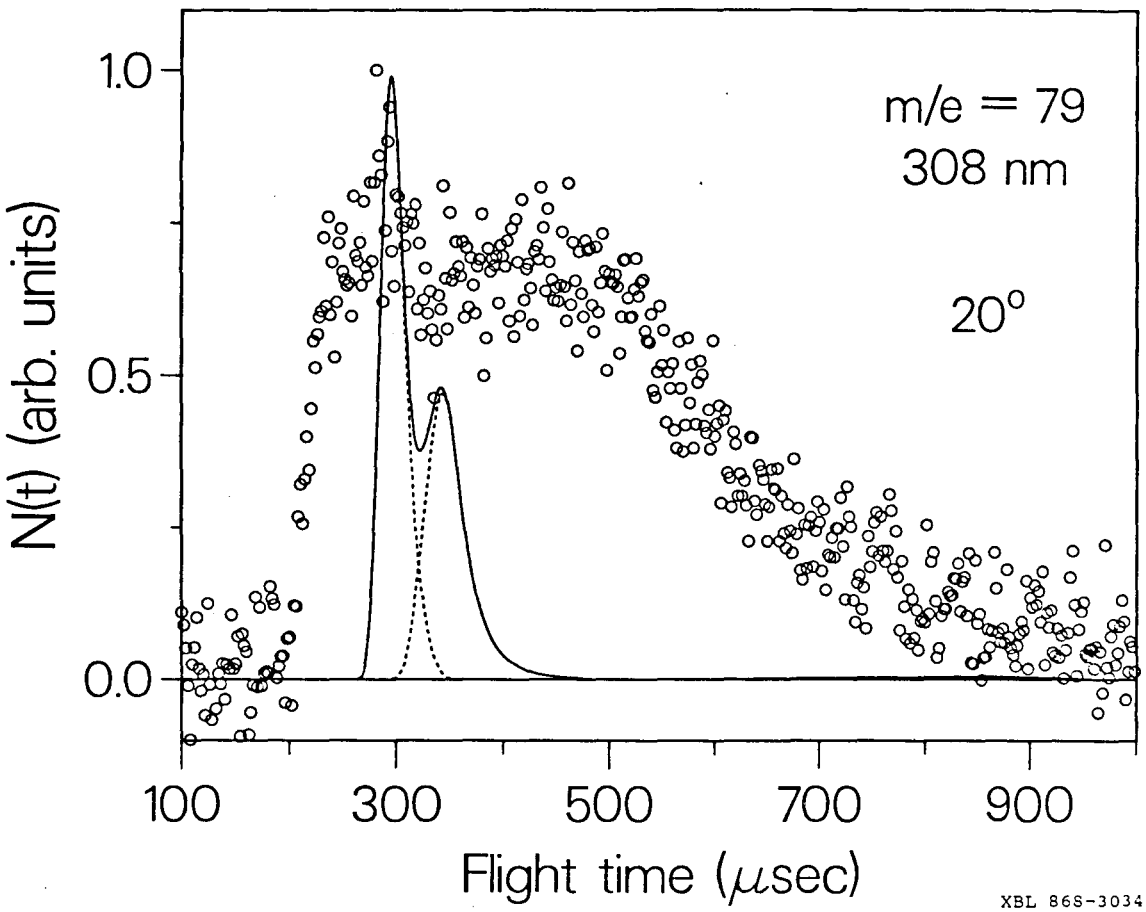
1.0
0.5
0.0
N(t) (arb. units)
m/e = 79
308 nm
20°
100
300
500
700
900
Flight time (μsec)
XBL 86S-3034

Figure 14

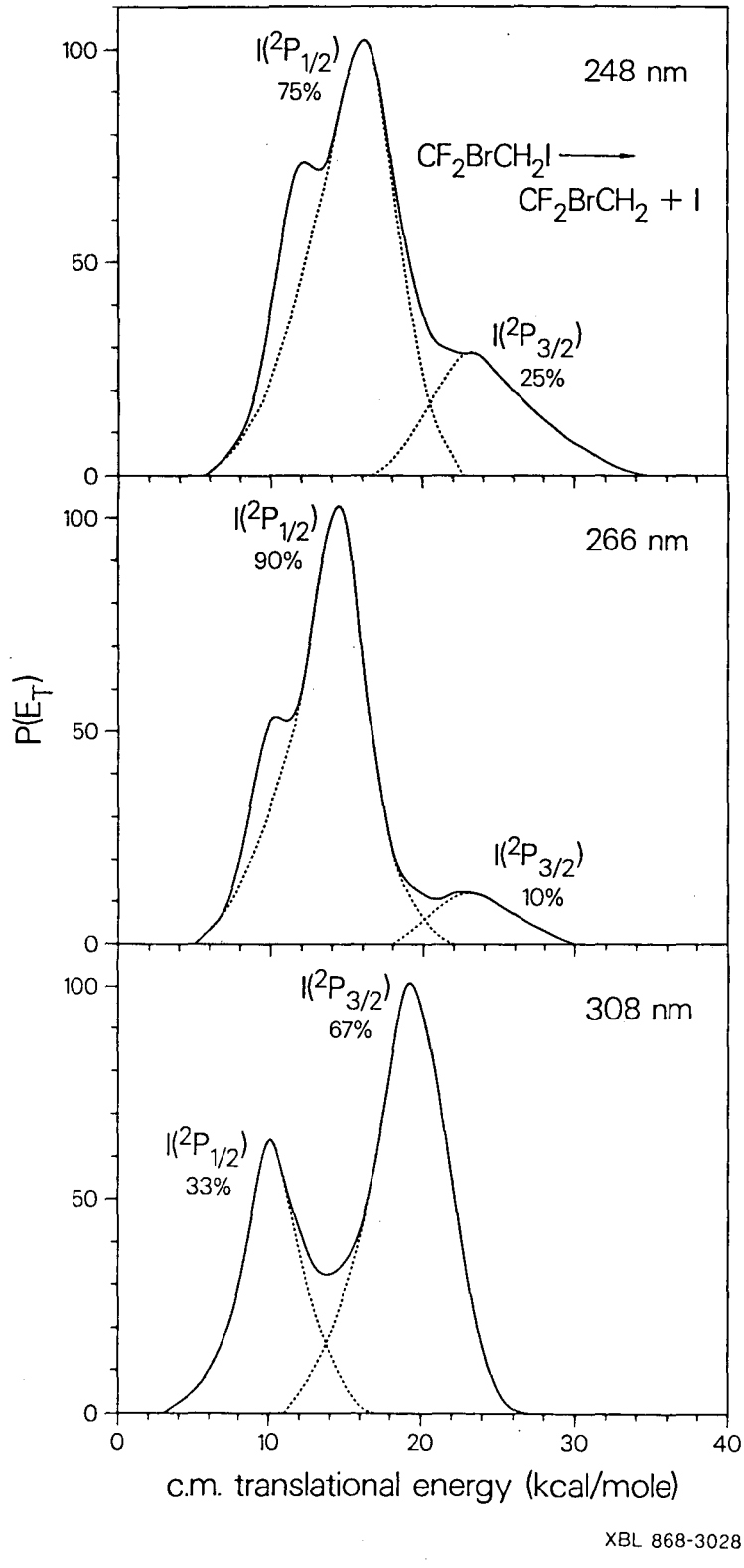
I(2P1/2)
75%
248 nm
CF2BrCH2I
CF2BrCH2 + I
I(2P3/2)
25%
I(2P1/2)
90%
266 nm
I(2P3/2)
10%
I(2P3/2)
67%
308 nm
I(2P1/2)
33%
P(ET)
100
50
0
0
10
20
30
40
c.m. translational energy (kcal/mole)
XBL 868-3028

Figure 15

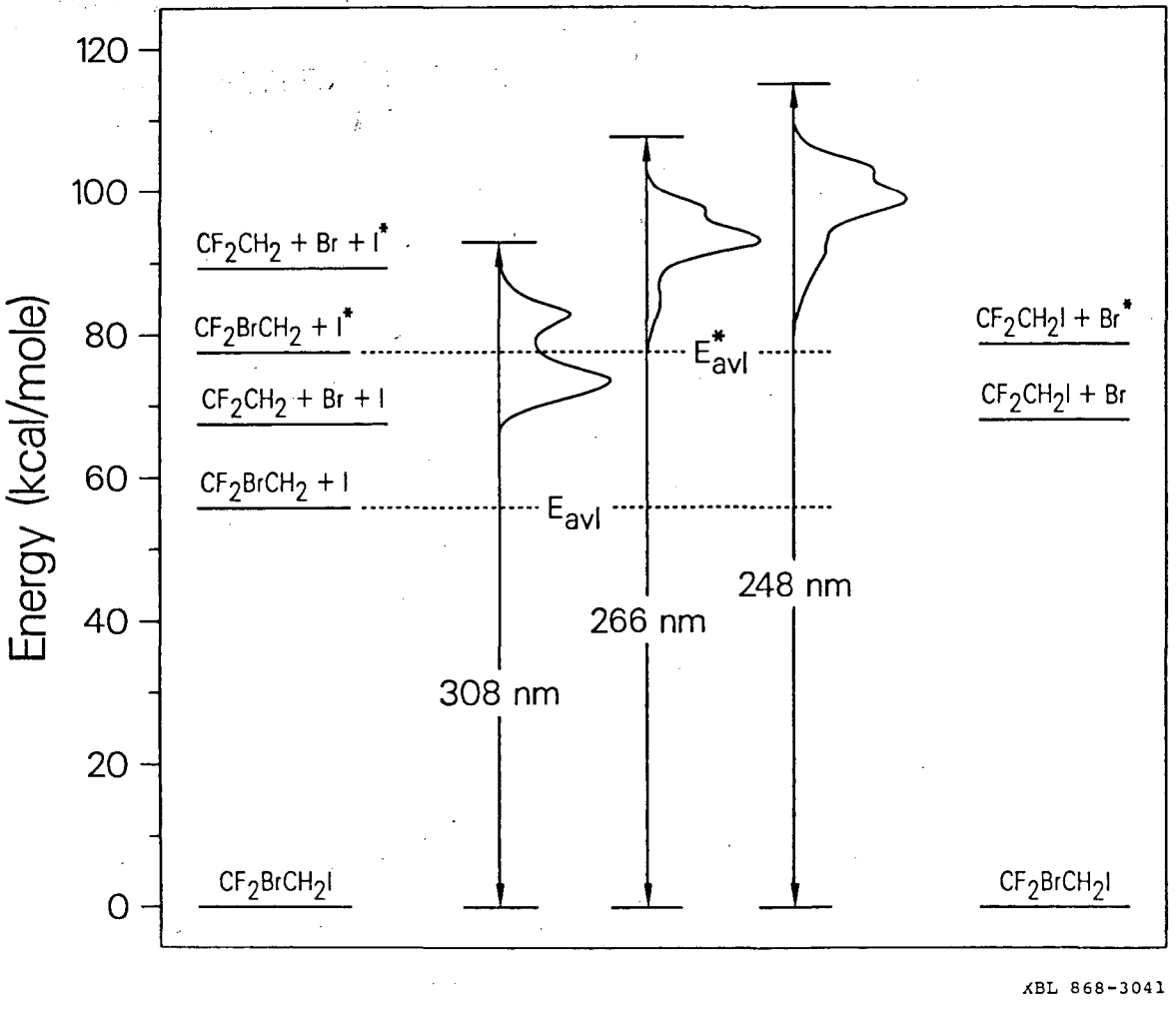
Energy (kcal/mole)
120
100
80
60
40
20
0
CF2CH2 + Br + I*
CF2BrCH2 + I*
CF2CH2 + Br + I
CF2BrCH2 + I
CF2BrCH2I
Eavl
E*avl
308 nm
266 nm
248 nm
CF2CH2I + Br*
CF2CH2I + Br
CF2BrCH2I
XBL 868-3041

Figure 16

This report was done with support from the Department of Energy. Any conclusions or opinions expressed in this report represent solely those of the author(s) and not necessarily those of The Regents of the University of California, the Lawrence Berkeley Laboratory or the Department of Energy.

Reference to a company or product name does not imply approval or recommendation of the product by the University of California or the U.S. Department of Energy to the exclusion of others that may be suitable.

LAWRENCE BERKELEY LABORATORY
TECHNICAL INFORMATION DEPARTMENT
UNIVERSITY OF CALIFORNIA
BERKELEY, CALIFORNIA 94720